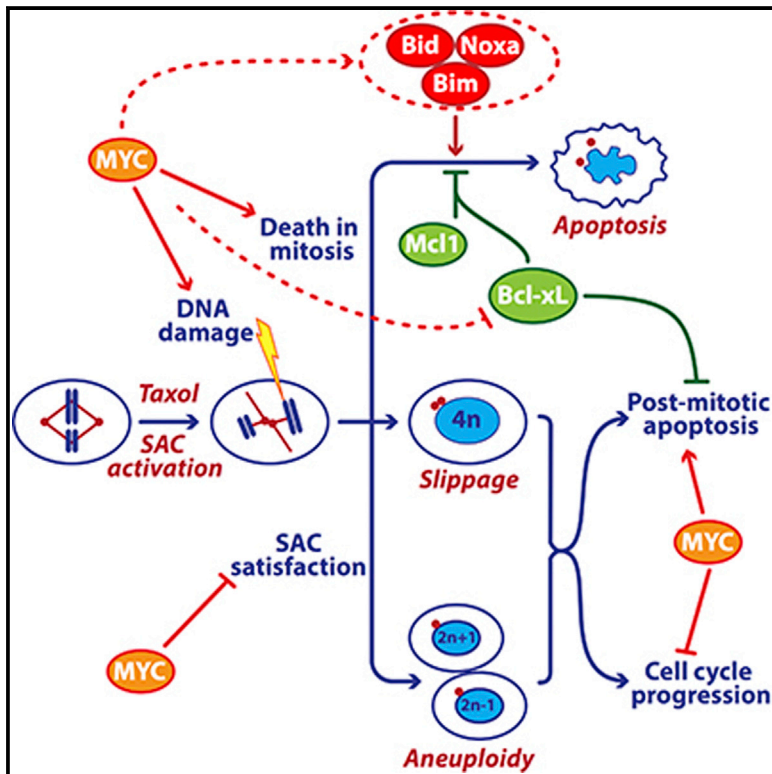


Cancer Cell

MYC Is a Major Determinant of Mitotic Cell Fate

Graphical Abstract



Highlights

- Genome-wide screen shows that Myc and Egr1 promote apoptosis during mitotic arrest
- Myc upregulates BH3-only proteins and downregulates Bcl-xL
- Myc sensitizes lung, breast, ovarian, and colon cancer cells to antimetabolic drugs
- Pharmacological inhibition of Bcl-xL restores apoptosis in Myc-low cells

Authors

Caroline Topham, Anthony Tighe, Peter Ly, ..., Owen J. Sansom, Don W. Cleveland, Stephen S. Taylor

Correspondence

stephen.taylor@manchester.ac.uk

In Brief

Topham et al. show that Myc sensitizes cancer cells to mitotic blockers and agents that accelerate mitotic progression by regulating the expression of an apoptotic network. Taxane responses in human breast cancers correlate positively with the Myc level and negatively with the Bcl-xL level.

Accession Numbers

GSE68219



MYC Is a Major Determinant of Mitotic Cell Fate

Caroline Topham,^{1,5} Anthony Tighe,^{1,5} Peter Ly,² Ailsa Bennett,¹ Olivia Sloss,¹ Louisa Nelson,¹ Rachel A. Ridgway,³ David Huels,³ Samantha Littler,¹ Claudia Schandl,¹ Ying Sun,² Beatrice Bechi,⁴ David J. Procter,⁴ Owen J. Sansom,³ Don W. Cleveland,² and Stephen S. Taylor^{1,*}

¹Faculty of Life Sciences, University of Manchester, Oxford Road, Manchester M13 9PT, UK

²Ludwig Institute for Cancer Research and Department of Cellular and Molecular Medicine, University of California at San Diego, La Jolla, CA 92093, USA

³Cancer Research UK Beatson Institute, Garscube Estate, Glasgow G61BD, UK

⁴School of Chemistry, University of Manchester, Oxford Road, Manchester M13 9PL, UK

⁵Co-first author

*Correspondence: stephen.taylor@manchester.ac.uk

<http://dx.doi.org/10.1016/j.ccell.2015.06.001>

This is an open access article under the CC BY-NC-ND license (<http://creativecommons.org/licenses/by-nc-nd/4.0/>).

SUMMARY

Taxol and other antimetabolic agents are frontline chemotherapy agents but the mechanisms responsible for patient benefit remain unclear. Following a genome-wide siRNA screen, we identified the oncogenic transcription factor Myc as a taxol sensitizer. Using time-lapse imaging to correlate mitotic behavior with cell fate, we show that Myc sensitizes cells to mitotic blockers and agents that accelerate mitotic progression. Myc achieves this by upregulating a cluster of redundant pro-apoptotic BH3-only proteins and suppressing pro-survival Bcl-xL. Gene expression analysis of breast cancers indicates that taxane responses correlate positively with Myc and negatively with Bcl-xL. Accordingly, pharmacological inhibition of Bcl-xL restores apoptosis in Myc-deficient cells. These results open up opportunities for biomarkers and combination therapies that could enhance traditional and second-generation antimetabolic agents.

INTRODUCTION

Antimetabolic drugs are frontline treatments for breast, ovarian, and lung cancer, as well as various hematological malignancies (Dumontet and Jordan, 2010). These drugs bind tubulin and inhibit microtubule dynamics, and although many cancers initially respond well, some are intrinsically resistant and others acquire resistance (Murray et al., 2012). Predicting which cancers will respond is hampered by our limited understanding of the molecular mechanisms responsible for patient benefit (Gascoigne and Taylor, 2009; Weaver, 2014). At high concentrations, antimetabolic drugs disrupt spindle assembly, leading to mitotic arrest by persistent activation of the spindle assembly checkpoint (SAC) (Lara-Gonzalez et al., 2012). SAC activation blocks the anaphase promoting complex/cyclosome (APC/C), thereby preventing ubiquitination and degradation of cyclin B1, in turn maintaining

the mitotic state. Following prolonged arrest, cells either die in mitosis or undergo “slippage,” returning to interphase without completing cell division (Brito and Rieder, 2006). Following slippage, p53-dependent post-mitotic responses then induce cell cycle arrest, senescence, or apoptosis (Rieder and Maiato, 2004). At lower taxol concentrations, the SAC becomes satisfied, allowing cells to progress through mitosis, albeit with spindle abnormalities and chromosome segregation errors (Zasadil et al., 2014). Bypassing both death in mitosis (DiM) and post-mitotic responses can fuel chromosome instability and taxane resistance (A'Hern et al., 2013).

The competing-networks model helps explain whether a cell either dies in mitosis or undergoes slippage (Gascoigne and Taylor, 2008). According to this model, two independent networks dictate mitotic cell fate, one slowly generating a death signal, the other slowly degrading cyclin B1, leading to slippage. During a

Significance

Antimetabolic agents such as the taxanes are used widely to treat various cancers. To address limitations with these agents, a new generation of inhibitors that disrupt mitosis without affecting microtubule dynamics is being evaluated, including drugs targeting mitotic kinesins and mitotic kinases. However, we still have limited understanding of the mechanisms that dictate cell fate in response to mitotic disruption. Here we show that Myc drives expression of an apoptotic network that sensitizes breast, ovarian, lung, and colon cancer cells to drugs that both activate and override the spindle assembly checkpoint. Moreover, we show that Myc promotes both p53-independent death in mitosis and p53-dependent post-mitotic responses. Our results raise opportunities to explore biomarkers and combination therapies aimed at enhancing antimetabolic efficacy.

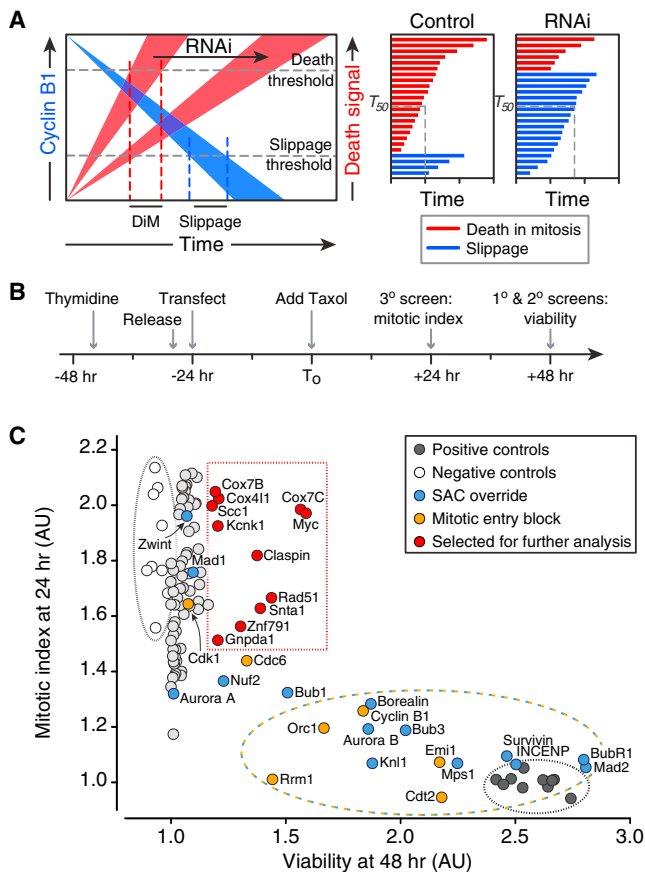


Figure 1. A Genome-wide siRNA Screen for Regulators of Mitotic Cell Fate

(A) Rationale for the screen based on the competing-networks model.

(B) Timeline of siRNA transfection procedure.

(C) Scatterplot of mitotic index at 24 hr against viability at 48 hr.

See also Figure S1 and Tables S1 and S2.

prolonged arrest, these networks work in opposite directions: while cell death signals become stronger, cyclin B1 levels slowly fall due to incomplete penetrance of SAC-mediated APC/C inhibition (Brito and Rieder, 2006). Both networks have thresholds and the fate of the cell is dictated by which threshold is breached first. Whereas our understanding of the mechanisms regulating cyclin B1 degradation is well advanced, less is known about death in mitosis. It involves the intrinsic apoptosis pathway; however, how this is regulated during mitosis is unclear (Topham and Taylor, 2013). The nature of the apoptotic trigger is also unclear, but DNA damage seems a likely candidate, with one source being partial activation of caspase-activated DNase (CAD), caused by cytochrome c leakage from mitochondria (Orth et al., 2012). A second source is telomere deprotection, driven by the mitotic kinase Aurora B (Hayashi et al., 2012). In light of our limited understanding regarding the mechanisms responsible for apoptosis during a mitotic arrest, we adopted an unbiased approach and screened a genome-wide library for siRNAs that suppress taxol-induced cell death. To define how genes identified in the screen modulate antimitotic responses, we then used single-cell time-lapse imaging to directly correlate mitotic behavior with subsequent cell fate.

RESULTS

A Genome-wide Screen for Regulators of Mitotic Cell Fate

The competing-networks model predicts that suppressing death signals during mitotic arrest provides more time for cyclin B1 degradation, thereby shifting cell fate from death to slippage (Figure 1A). To test this, we screened an siRNA library to identify genes required for DiM. Because slippage results in cell survival, we based the screen on a viability assay (Figure S1A). To maximize the assay's dynamic range, we treated RKO cells, which predominantly undergo DiM (Gascoigne and Taylor, 2008), with a saturating concentration of taxol to ensure maximal mitotic blockage and apoptotic response. We also synchronized the cells to maximize cell death by 48 hr (Figure 1B). The primary screen identified 325 hits (Figure S1B). To filter out off-target hits, we performed a secondary screen using a pool of four different siRNAs, yielding 100 hits. Because taxol-induced death requires mitotic entry and robust spindle checkpoint activation, we predicted that in addition to DiM genes, the screen would also uncover genes required for cell cycle progression and SAC function. Indeed, we identified all the known SAC components, several kinetochore proteins required for SAC function and the entire chromosomal passenger complex, plus several genes required for mitotic entry (Figure 1C). To distinguish cell cycle and SAC genes from potential DiM genes, we performed a tertiary screen measuring mitotic index at 24 hr (Figure 1B) and plotted it against viability at 48 hr (Figure 1C). To hone in on potential DiM genes, we focused on hits with a high mitotic index at 24 hr and a substantial viability score at 48 hr (Figure 1C). Time-lapse microscopy showed that siRNA pools targeting *KCNK1*, *ZNF791*, *SNTA1*, and *MYC* shifted cell fate from death to slippage (Figure S1C). Importantly, mitotic exit was not accelerated, indicating inhibition of apoptosis rather than SAC override.

Myc Is a Regulator of Cell Fate following Prolonged Mitotic Arrest

Of the four hits, we first focused on *MYC*, which encodes the bHLH-Zip transcription factor c-Myc (hereafter Myc). Myc, a potent oncogene deregulated in many cancers, regulates a multitude of genes via both transcriptional amplification and co-factor-dependent activation/repression (Conacci-Sorrell et al., 2014; Eilers and Eisenman, 2008; Hann, 2014; Wolf et al., 2015). Myc thus drives numerous biological pathways including proliferation, biogenesis, and metabolism which, when deregulated, promote transformation and tumorigenesis. Because Myc can also drive apoptosis, primarily via the ARF-MDM2-p53 pathway (Lowe et al., 2004; McMahon, 2014), we considered it an attractive candidate for a DiM gene. To validate Myc as a bona fide on-target hit, we deconvolved the siRNA pools, identifying four distinct siRNAs that repressed Myc and inhibited DiM (Figures S1D and S2A). When combined, these four siRNAs reduced Myc protein levels by 90% and shifted cell fate in favor of slippage (Figures 2A and 2B). In nine control experiments, quantitating 100 cells per population, 82% of cells underwent DiM, while 18% slipped (Figure 2C). In five Myc RNAi populations, 45% of cells died, while 55% slipped. Moreover, titrating the siRNAs revealed a correlation between Myc protein levels and cell fate (Figure 2D). In addition, an RNAi-resistant Myc transgene

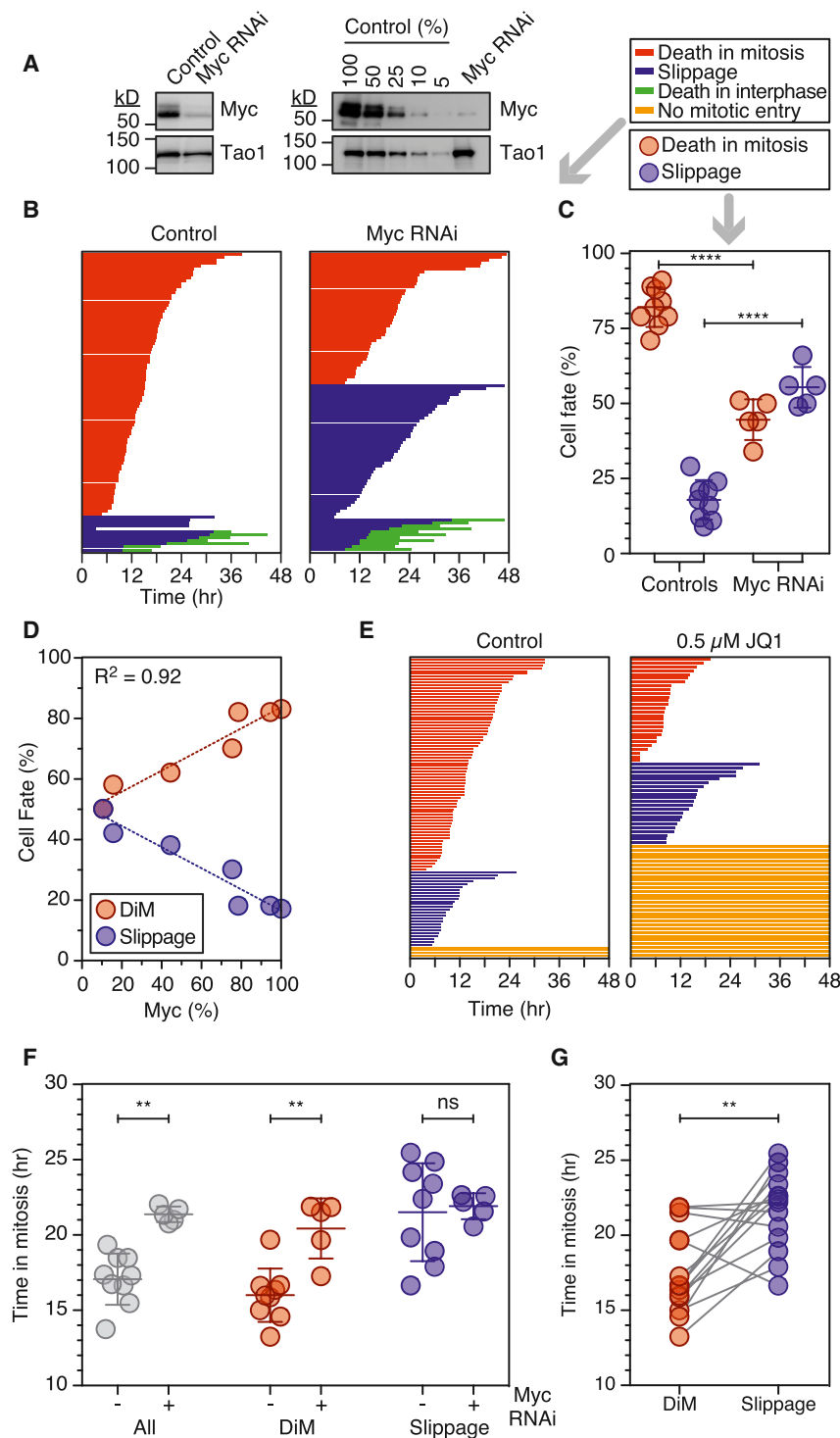


Figure 2. Myc Is a Regulator of Mitotic Cell Fate

(A) Immunoblots showing Myc inhibition. (B) Fate profiles of RKO cells exposed to 0.1 μ M taxol following Myc RNAi. (C) Cell fate in nine control and five Myc RNAi populations. (D) Correlation between Myc protein levels and cell fate. (E) Fate profiles of RKO cells exposed to 0.1 μ M taxol and 0.5 μ M JQ1. (F) Time spent arrested in mitosis; entire population (gray), cells that die (red), and cells that slip (blue). (G) Time arrested in mitosis with lines connecting cells from the same population. **p < 0.01, ****p < 0.0001. See also Figure S2.

(Filippakopoulos et al., 2010; McKeown and Bradner, 2014) and accordingly JQ1 inhibited Myc expression in RKO cells (Figure S2C). This was accompanied by a substantial effect on proliferation (Figure 2E). However, of the cells that did enter mitosis, only 56% were killed by taxol, demonstrating a shift in favor of slippage (Figure 2E). Significantly, a Myc cDNA resisted the DMSO and JQ1 effects and restored DiM (Figure S2D). To determine whether Myc's role in DiM depends on its ability to modulate gene expression, we turned to Omomyc, a mutant bHLH-Zip domain that sequesters Myc in complexes unable to bind to E-boxes (Soucek et al., 2002). Inducing Omomyc in RKO cells inhibited DiM (Figure S2B), indicating that Myc most likely promotes DiM via its canonical role as a transcription factor. Interestingly Myc V394D, which cannot bind the Miz1 transcriptional repressor (Wiese et al., 2013), rescued Myc RNAi (Figure S2B), suggesting that Myc promotes DiM largely via transcriptional activation. Taking together the RNAi data, the DMSO, JQ1, and Omomyc experiments, we conclude that Myc is a key determinant of cell fate following prolonged mitotic arrest.

Using Myc to Test the Competing-Networks Model

The competing-networks model predicts that suppressing mitotic death provides

reverted the fate profile back toward DiM (Figure S2B). To further validate Myc, we turned to non-RNAi modalities, in particular the small molecules DMSO and JQ1 (Figure S2C). DMSO, which blocks transcriptional elongation of MYC (Eick and Bornkamm, 1986), efficiently suppressed Myc in RKO cells (Figure S2C) and reduced DiM from 92% to 58% (Figure S2D). JQ1 displaces the Brd4 transcriptional elongation factor from the MYC promoter

more time for cyclin B1 degradation, thus shifting the balance toward slippage. A corollary is that the average time spent in mitosis should increase (Figure 1A). Consistently, whereas controls spent 17.1 hr arrested in mitosis, Myc-deficient cells spent 21.3 hr (Figure 2F) arrested in mitosis. Moreover, when we compared the cells that died, controls took 16.0 hr, whereas Myc-deficient cells took 20.4 hr; thus, even if a cell did not

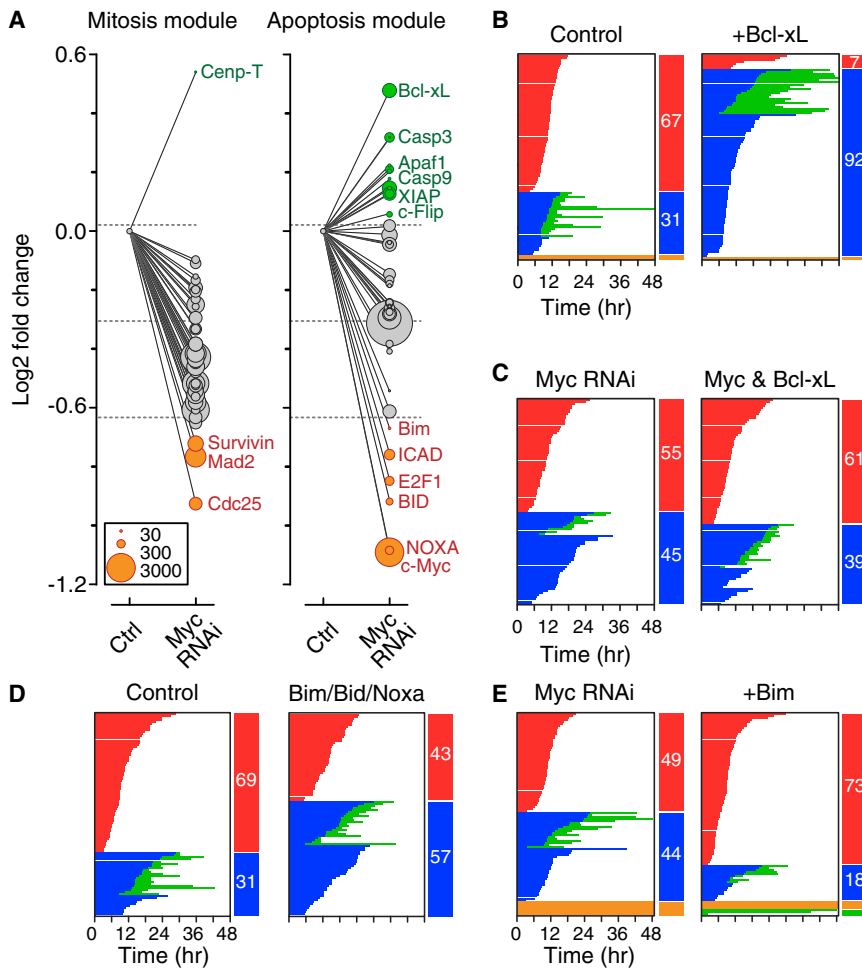


Figure 3. A Cluster of Redundant BH3-Only Proteins Promote Death in Mitosis

(A) Gene expression changes following Myc RNAi; y axis shows the fold change and circle sizes reflect the number of transcripts detected. Horizontal lines represent mean \pm 1 SD.

(B–E) Fate profiles of RKO cells exposed to 0.1 μ M taxol following tet-induced overexpression of Bcl-xL (B); RNAi-mediated co-repression of Myc and Bcl-xL (C); RNAi-mediated co-repression of Bim, Bid, and Noxa (D); and tet-induced overexpression of Bim following Myc RNAi (E). See also Figure S3 and Table S3.

Myc RNAi promotes survival, the dominant effectors are likely to be upregulated pro-survival genes and/or downregulated pro-death genes. Of the upregulated genes, Bcl-xL is a well-established pro-survival factor, while three of the downregulated genes, namely Bid, Bim, and Noxa, encode BH3-only pro-apoptotic proteins (Figure 3A). Because these are Myc effectors in other contexts (McMahon, 2014), we analyzed them in more detail.

BH3-Only Pro-apoptotic Proteins Are Redundant Effectors of Myc

Consistent with Myc's known ability to repress Bcl-xL (Eischen et al., 2001), Myc RNAi elevated Bcl-xL protein levels in RKO cells (Figure S3B). Ectopic overexpression of Bcl-xL suppressed both DiM and post-mitotic apoptosis (Figures

3B and S3C), supporting the notion that Bcl-xL is a potent mitotic survival factor (Bah et al., 2014; Minn et al., 1996; Upreti et al., 2008). However, ectopic Bcl-xL enhanced survival more potently than Myc RNAi, suggesting that other consequences of Myc inhibition attenuate the pro-survival effect of increased Bcl-xL (Eichhorn et al., 2014). Indeed, whereas Mcl1 transcripts fell only marginally upon Myc RNAi, Mcl1 protein levels fell substantially (Figures S3B and S3E), possibly due to deregulation of factors involved in Mcl1 turnover. However, in taxol-arrested cells, this residual Mcl1 appeared to resist mitotic degradation (Figure S3E). Nevertheless, despite these complexities, we reasoned that Bcl-xL upregulation alone is unlikely to explain the Myc RNAi phenotype, and therefore we turned our attention to the downregulated pro-death genes.

Myc Inhibition Deregulates an Apoptosis Module

To define how Myc promotes DiM, we interrogated mitosis and apoptosis gene expression modules using Nanostring technology. With the exception of Cenp-T, all the mitosis genes were suppressed following Myc RNAi (Figure 3A), reflecting Myc's role as a transcriptional amplifier and/or cell cycle driver. Of the three notably repressed genes, Survivin and Mad2 promote chromosome alignment and SAC function. Consistently, in the absence of taxol, whereas overall mitotic timing was normal in Myc RNAi cells, chromosome alignment was delayed slightly and anaphase onset slightly accelerated (Figure S3A). Nevertheless, despite these subtle effects on an unperturbed mitosis, Figure 2 clearly demonstrates that Myc-deficient cells mount a robust SAC response in 100 nM taxol, suggesting that mitotic deregulation is unlikely to account for the shift in cell fate. We therefore turned to the apoptosis module, which included 12 upregulated and six downregulated genes (Figure 3A). Because

escape death, inhibiting Myc delayed its onset. Slippage typically took longer than DiM (Figure 2G) and the time from mitotic entry to slippage was not significantly affected by Myc RNAi (Figure 2F), consistent with the notion that the two competing networks are independent, and that Myc influences the death pathway but not the slippage pathway.

The downregulated BH3-only proteins (Figure 3A), namely Bid, Bim, and Noxa, are known to be upregulated by Myc, either directly or via the ARF-MDM2-p53 pathway (McMahon, 2014). If Bid, Bim, and Noxa are important Myc DiM effectors, then their inhibition should mimic Myc RNAi. However, because they did not manifest in the screen they are unlikely to be essential for DiM. Indeed, repression of each in isolation or in pairs had little effect on mitotic fate (Figure S3G). In contrast, co-repression of Bim, Bid, and Noxa tipped the balance in favor of slippage (Figure 3D), consistent with them being redundant

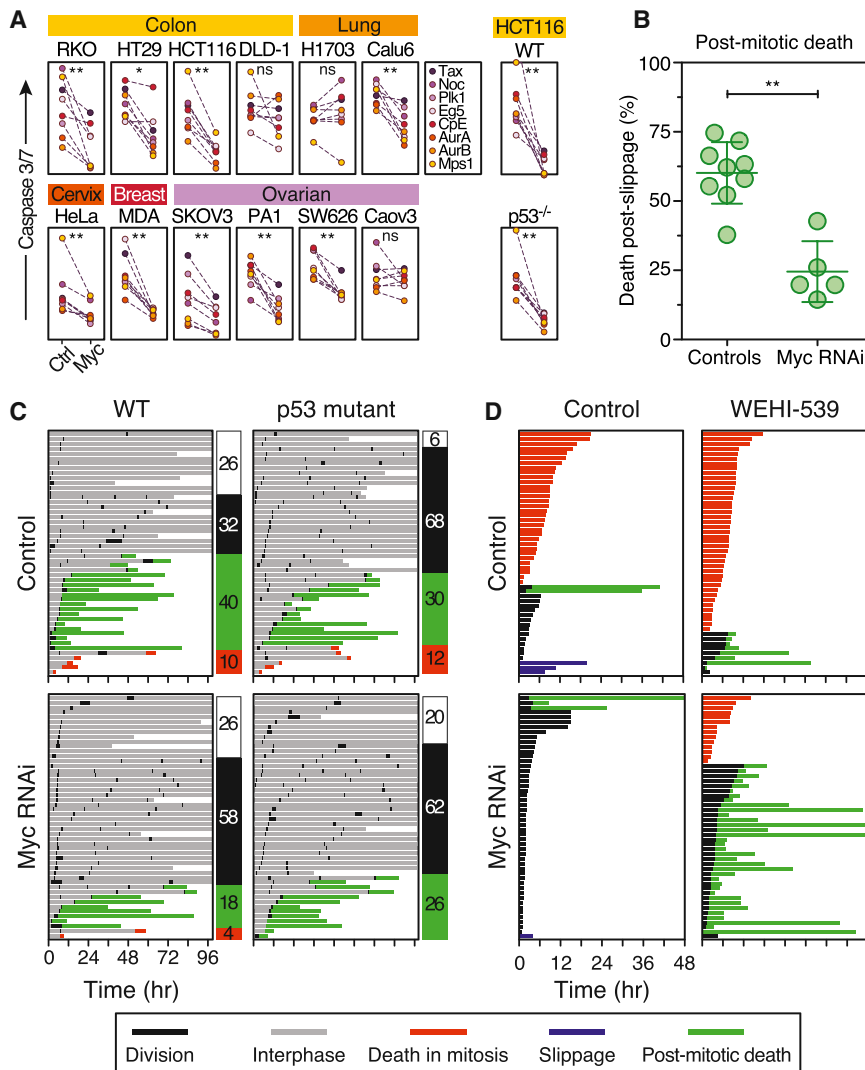


Figure 4. Myc Promotes Post-mitotic Death

(A) Apoptosis induction in cell lines indicated exposed to various antimetabolic agents following Myc RNAi.

(B) Graph quantitating death following slippage in the presence of 0.1 μ M taxol.

(C) Fate profiles of wild-type and p53-deficient HCT116 cells following Myc RNAi then exposed to the Mps1 inhibitor AZ3146 (2 μ M). Numbers indicate percentage of cells that undergo one division (white), multiple divisions (black), post-mitotic death (green), and DiM (red).

(D) Fate profiles of RKO cells exposed to 10 nM taxol in combination with 100 nM WEHI-539. In (C), 0 hr is when imaging started. * $p < 0.05$, ** $p < 0.01$. See also Figure S4 and Table S4.

ceptions. DLD-1 cells slip very quickly (Gascoigne and Taylor, 2008); therefore, despite inhibiting DiM, slippage would be expected to continue such that Myc RNAi has little effect. Conversely, H1703 cells die very quickly and rarely slip, suggesting that despite delaying DiM, slippage may not be fast enough to permit exit. Nevertheless, Myc promotes apoptosis in a variety of cancer lines exposed to various antimetabolic agents.

MYC Promotes Apoptosis following Slippage

In contrast to taxol, drugs targeting Aurora B and Mps1 drive cells through an aberrant mitosis (Keen and Taylor, 2009), suggesting that Myc also promotes apoptosis following slippage. Indeed, following exit from a prolonged taxol arrest, Myc RNAi reduced cell

downstream effectors of Myc. A corollary is that overexpression of any one should revert the Myc RNAi phenotype. Indeed, transgenic Bim restored DiM in Myc RNAi cells (Figures S3E and S3H). Consistent with the competing-networks concept, Bim/Bid/Noxa RNAi extended mitotic timing, whereas induction of Bim accelerated the onset of DiM (Figure S3I). We conclude therefore that Bim, Bid, and Noxa are redundant Myc effectors required for DiM.

MYC Sensitizes Various Cancer Lines to Antimetabolic Drugs

To test the role of Myc in a wider context, we inhibited Myc in 12 cell lines derived from colon, lung, breast, cervical, and ovarian cancers (Figure S4A), then exposed them to a panel of antimetabolic drugs including agents targeting Eg5/KSP, Plk1, Cenp-E, Aurora A, Aurora B, and Mps1. To monitor apoptosis, we used time-lapse imaging to measure caspase-3/7 activity. The effects of inhibiting Myc were strikingly consistent, significantly attenuating apoptosis in nine lines (Figure 4A). Interestingly, Myc inhibition had little effect in three lines, namely DLD-1, H1703, and Caov-3. The competing-networks model may explain these ex-

death from 60% to 25% (Figure 4B). Moreover, in response to an Mps1 inhibitor, Myc RNAi reduced post-mitotic apoptosis from 40% to 18% (Figure 4C) and enhanced colony formation (Figure S4B). Canonical Myc-driven apoptosis involves the ARF-MDM2-p53 pathway; however, because p53 is disengaged during mitosis, Myc-dependent DiM is likely p53-independent. Indeed, Myc RNAi suppressed apoptosis in p53-deficient HCT116 cells treated with mitotic blockers (Figure 4A). Consistent with p53 restraining further cell cycle progression following an aberrant mitosis (Thompson and Compton, 2010), p53 deletion increased the number of HCT116 cells entering a second mitosis from 32% to 68% (Figure 4C). However, apoptosis was only slightly affected by p53 loss, 30% versus 40% in controls, indicating that post-mitotic apoptosis is largely p53-independent. Interestingly, whereas Myc RNAi only had a marginal effect on post-mitotic apoptosis in p53-deficient cells, it increased the number of p53-proficient cells entering a second mitosis from 32% to 58% (Figure 4C). Thus, following an aberrant mitosis, Myc not only enhances post-mitotic apoptosis but also suppresses cell cycle progression, possibly via the ARF-MDM2-p53 pathway.

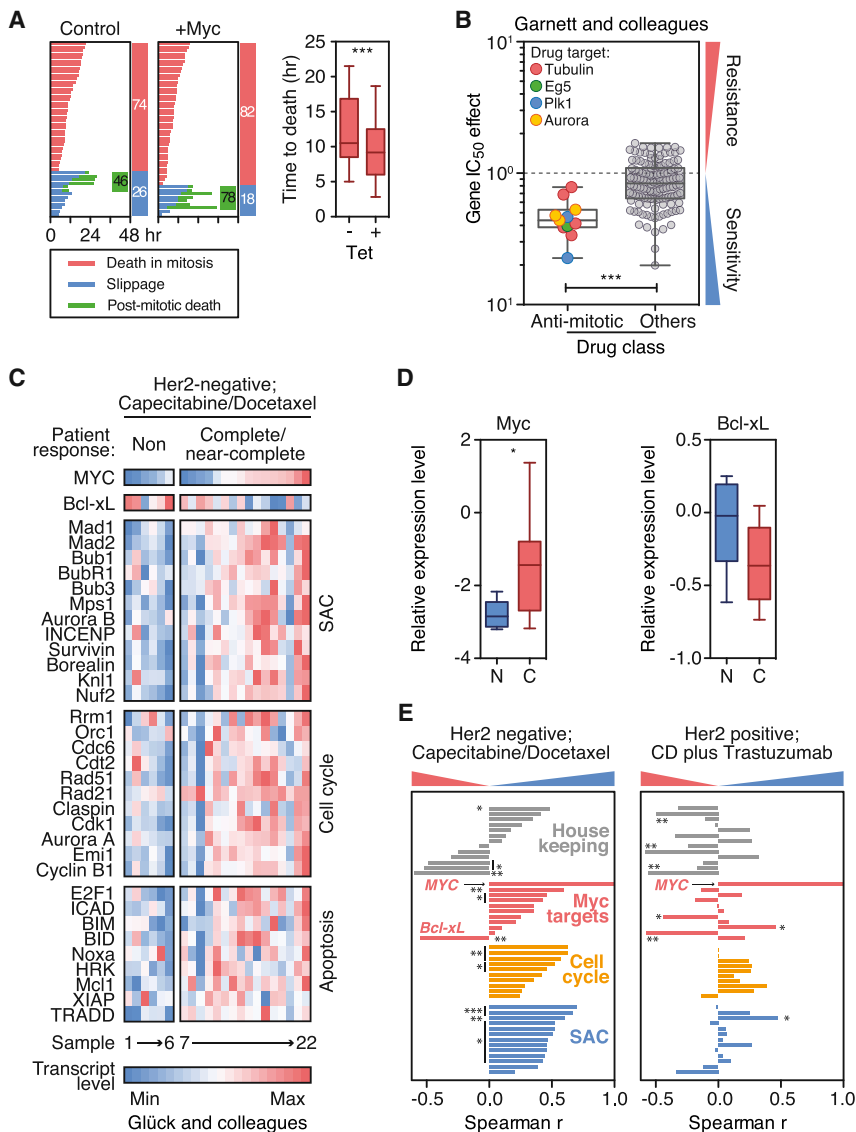


Figure 5. Overexpression of Myc Sensitizes Cancer Cells to Antimitotic Agents

(A) Fate profiles and box-and-whisker plot showing time to DIM in RKO cells exposed to 0.1 μ M taxol following tet-induced overexpression of Myc.

(B) Gene IC₅₀ effects for MYC comparing antimitotic agents with other drugs.

(C) Heatmaps showing gene expression profiles of 22 breast tumors (six non-responders and 16 complete/near-complete responders) treated with capecitabine and docetaxel.

(D) Box-and-whisker plots showing Myc and Bcl-xL expression levels in non-responsive (N) and responsive tumors (C).

(E) Bar graphs showing correlations between MYC and the SAC, cell cycle, and apoptosis genes. * $p < 0.05$, ** $p < 0.01$, *** $p < 0.001$.

See also Figure S5 and Tables S5 and S6.

indeed, when we added 100 nM WEHI-539, a selective Bcl-xL inhibitor (Lessene et al., 2013), all the cells that divided subsequently died (Figures 4D and S4C). Thus, inhibiting Myc enhances survival in low-dose taxol but this can be ameliorated by inhibition of Bcl-xL.

Tumor Cells Overexpressing MYC Are Sensitive to Antimitotic Agents

Because inhibiting Myc suppresses apoptosis in response to antimitotic agents, we asked whether elevating Myc expression had the opposite effect. Indeed, tet-induction of a Myc transgene in RKO cells accelerated DIM by 2.3 hr and reduced slippage, albeit modestly (Figure 5A). Moreover, of the cells that slipped, overexpressing Myc increased post-mitotic death from 46% to 78%. Consistently, overexpressing Myc in

Rat1a cells enhances colcemid-induced apoptosis (Li and Dang, 1999). To examine Myc overexpression in a wider context, we interrogated the Genomics of Drug Sensitivity in Cancer database (Garnett et al., 2012), which describes 665 cell lines, 47 of which overexpress Myc, in response to 141 drugs, 11 of which target microtubules or mitotic regulators. The mean half-maximal inhibitory concentration (IC₅₀) effect for the 11 antimitotic drugs was 0.47 compared to 0.83 for the other 130 drugs (Figures 5B and S5A), confirming that tumor cells overexpressing Myc are more sensitive to antimitotic agents compared to drugs in general.

To determine whether the Myc overexpression effect extended to patient chemotherapy responses, we interrogated microarray datasets from XeNA, a clinical trial examining response rates in women with operable, early stage breast cancer receiving neoadjuvant capecitabine plus the antimitotic agent docetaxel (Glück et al., 2012). Tumors from patients showing complete or near-complete responses tended to have elevated Myc (Figures 5C and 5D). Next, we analyzed the SAC

Myc Enhances Survival in Low-Dose Taxol

In breast cancers, taxol does not accumulate to concentrations high enough to induce prolonged mitotic arrest; rather cells progress through mitosis, albeit with chromosome segregation errors (Zasadil et al., 2014). Because Myc promotes post-mitotic death, we reasoned that Myc would also influence low-dose taxol responses. To test this, we reduced the taxol concentration to 10 nM (Figure S4C), a concentration in cell culture medium that results in intracellular concentrations similar to those measured in breast cancer (Zasadil et al., 2014). In 10 nM taxol, most RKO cells died in mitosis but 31% divided, indicating that the taxol concentration was “on the edge” (Figure 4D). Of those that divided, 12.5% died in the next interphase. Strikingly, Myc RNAi cells spent considerably less time in mitosis then divided, indicating that the SAC became satisfied (Figure 4D). Consistently, Myc RNAi slightly accelerated anaphase onset during an unperturbed mitosis (Figure S3A). Following division in 10 nM taxol, Myc RNAi cells survived, at least for the duration of the experiment. These divisions are unlikely to be normal;

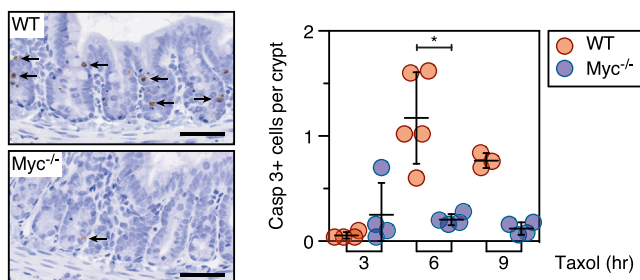


Figure 6. MYC-Deficient Crypts Are Resistant to Taxol-Induced Apoptosis

Immunohistochemical staining and quantitation of cleaved caspase 3 in intestinal sections from wild-type and MYC mutant mice following 3, 6, and 9 hr exposure to taxol. Bar represents 50 μm . * $p < 0.05$.

and cell cycle genes identified by the siRNA screen (Figure 1C), and the Myc regulated genes identified by our Nanostring analysis (Figure 3A). Although there was no obvious overall correlation between Myc and several housekeeping genes, Myc correlated positively with the SAC, cell cycle, and apoptosis genes (Figures 5C and 5E). Moreover, the SAC, cell cycle, and Myc clusters were elevated in the responsive tumors (Figure S5B). The elevation was not simply due to a global increase in gene expression because Bcl-xL displayed a negative correlation (Figures 5C–5E), consistent with Myc-induced suppression (Figure 3A). Moreover, the correlation between Myc and cell cycle/SAC genes was not simply due to increased proliferation, because Her2-positive tumors did not show a similar pattern (Figures 5E and S5C). These results suggest that a positive response to antimetabolic chemotherapy requires entry into mitosis, a robust SAC response, and the ability to undergo Myc-dependent apoptosis.

Myc Is Required for Taxol-Induced Apoptosis in Mouse Intestinal Crypts

The correlation between Myc expression and chemotherapy responses is provocative. However, Her2-negative breast cancers include various tumor subtypes and XeNA used multiple chemotherapy agents. We therefore turned to a genetically constrained model system that allows single agent exposure to validate the role of Myc in the context of an intact tissue. Mice harboring a conditional MYC allele provided such a system (Pheesse et al., 2014). *AhCre⁺ MYC^{fl/fl}* mice were injected with β -naphthoflavone to delete MYC in the small intestine. Four days later, taxol was administered to induce mitotic arrest and then apoptosis was measured with caspase 3 staining (Radulescu et al., 2010). In Myc-deficient intestines, we observed 0.2 apoptotic cells per intestinal crypt compared to 1.2 in Myc-proficient controls (Figure 6). We conclude therefore that Myc is a determinant of mitotic cell fate in the mouse intestine.

Interrogating Kcnk1, Snta1, and Znf791

The transcript profiling and functional experiments indicate that Myc enhances DiM by suppressing Bcl-xL and upregulating BH3-only proteins (Figure 3). However, a defining feature of Myc is its ability to modulate numerous genes thereby influencing various biological processes, including biosynthesis

and metabolism pathways (Conacci-Sorrell et al., 2014; Eilers and Eisenman, 2008). Consequently, Myc targets not included in the Nanostring analysis could contribute to the phenotype. Moreover, the screen identified *KCNK1*, *ZNF791* and *SNTA1* (Figure S1C), but it is not immediately obvious how they might modulate apoptosis. To address these issues, we deconvolved the *Kcnk1*, *Znf791*, and *Snta1* siRNA pools. In each case, only a single siRNA sequence enhanced viability, suggesting that they were “off-target” hits (Figure S1D). When transfected in isolation, the active *Znf791* and *Snta1* siRNAs accelerated mitotic exit rather than delaying DiM (Figure S1E). In contrast, the active *Kcnk1* siRNA induced a Myc-like phenotype, suppressing DiM without accelerating mitotic exit. Therefore, to identify the target of this siRNA, and to interrogate Myc target genes not included in the Nanostring analysis, we turned to global gene expression profiling.

Egr1 Promotes Death in Mitosis

RKO cells were transfected with Myc, *Kcnk1*, and *Snta1* siRNAs and then cDNA libraries were sequenced using Illumina HiSeq technology. Myc RNAi induced numerous changes, with 955 downregulated genes and 1,214 upregulated genes (Figure 7A). The effect on Myc itself was relatively modest, possibly reflecting negative auto-regulation (Conacci-Sorrell et al., 2014). Gene ontology analysis highlighted ribosome biogenesis, metabolism, gene expression, cell cycle, and apoptosis pathways (Figure S6C), consistent with known Myc functions. The *Kcnk1* siRNA affected 424 genes, with *KCNK1* itself one of the most repressed (Figure 7A). Whereas gene ontology analysis also highlighted metabolism and biosynthesis pathways, the p values and fold enrichment scores were substantially lower (Figure S6C), indicating that DiM can be suppressed without major effects on metabolism and biosynthesis pathways.

To understand how the active *Kcnk1* siRNA suppresses DiM, we focused on the 58 downregulated genes in common with Myc (Figure 7B). Only two were repressed more than 2-fold in both conditions, namely *SNORD102* and *EGR1*. Of these, *Egr1*, a zinc finger transcription factor, stands out as it is an established Myc target required for Myc-dependent, p53-independent apoptosis, and it cooperates with Myc to upregulate *Bim* and *Noxa* (Boone et al., 2011; Wirth et al., 2014). We reasoned therefore that the *Kcnk1* siRNA might suppress DiM via inhibition of *Egr1*. Consistently, transcript profiling indicated that *Bim*, *Bid*, and *Noxa* were reduced following *Kcnk1* siRNA (not shown). To test directly whether *Egr1* promotes DiM, we transfected RKO cells with siRNAs specifically targeting *Egr1*. Strikingly, this shifted cell fate from DiM to slippage in a manner comparable to Myc siRNA (Figure 7C). Thus, these observations identify *EGR1* as a “DiM” gene and suggest that *KCNK1* manifested in the screen because of off-target activity toward *Egr1*.

Myc Modulates DNA Damage Accumulation in Mitosis

Although Myc and *Egr1* appear to set the stage for DiM, what actually triggers apoptosis during a prolonged mitotic arrest is unclear. During the course of this work, we made two observations suggesting that Myc may modulate two recently identified mechanisms (Hayashi et al., 2012; Orth et al., 2012). First, we noted that ICAD, the inhibitor of CAD, was markedly reduced by Myc RNAi (Figure 3A). This was intriguing in light of the demonstration

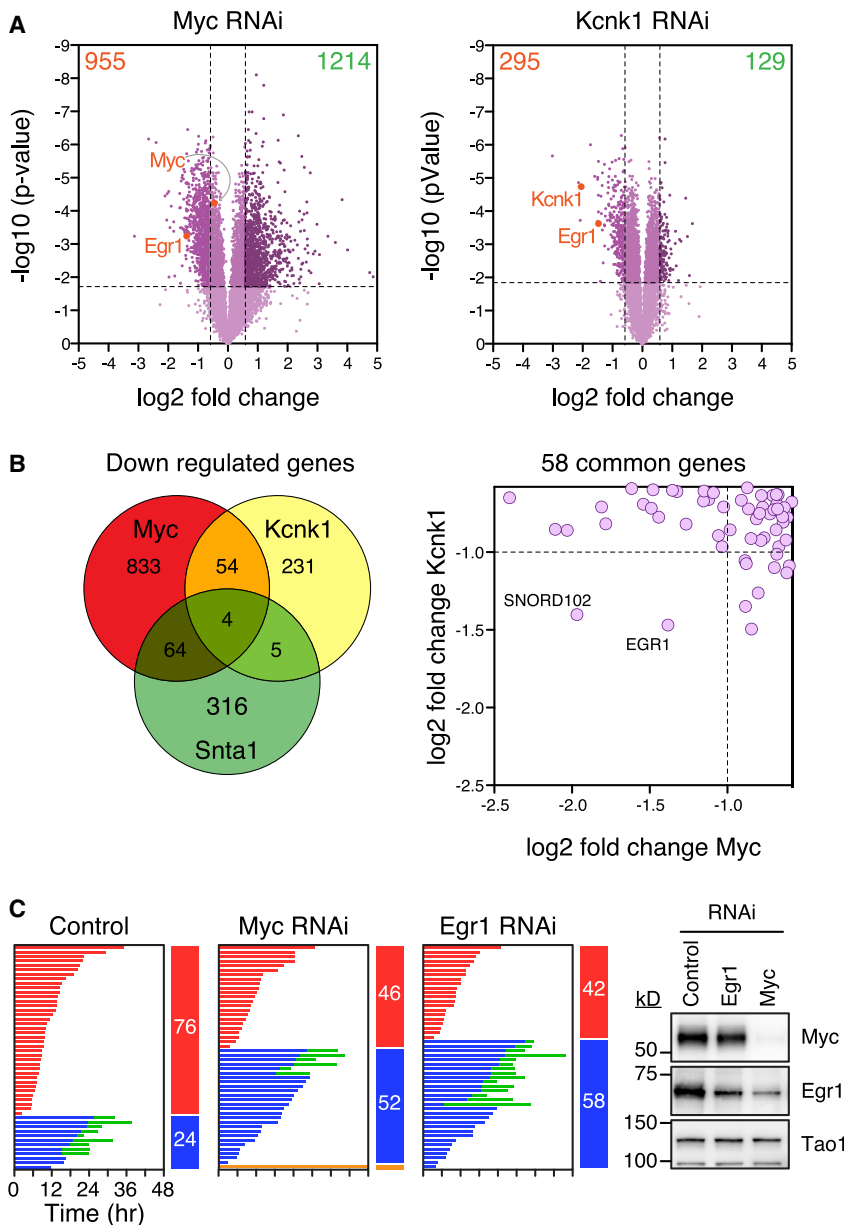


Figure 7. Egr1 Is a Regulator of Mitotic Cell Fate

(A) Volcano plots showing gene expression changes following Myc and Kcnk1 RNAi.

(B) Venn diagram and scatterplot showing common downregulated genes.

(C) Fate profiles of RKO cells exposed to 0.1 μ M taxol following Egr1 RNAi and immunoblots showing reduced Egr1 following Myc RNAi.

See also Figure S6 and Table S7.

Bcl-xL and Mcl1 (not shown). In contrast, telomere deprotection might cause a burst of DNA damage upon mitotic entry (Hayashi et al., 2012). Indeed, inhibiting Aurora B in Bcl-xL/Mcl1-deficient cells reduced DiM from 69% to 34% (Figure S7C) and suppressing telomere deprotection by overexpressing TRF2 also had a protective effect (Figures 8B and S7D). Inhibiting Myc in Bcl-xL/Mcl1-deficient cells had an even more penetrant effect, reducing DiM in the absence of taxol from 69% to 10% (Figure S7C). Although this could simply reflect Myc's role setting the balance between pro-survival and pro-death factors, these observations raise the possibility that Myc may also modulate the DNA damage-inducing pathways that trigger apoptosis during a prolonged mitotic arrest.

DISCUSSION

The success of the siRNA screen was predicated on the existence of genes essential for DiM. Consistent with the SAC being indirectly required for DiM (Taylor and McKeon, 1997), we identified all the known SAC components. Indeed, SAC genes frequently manifest in antimetabolic RNAi screens, yet apoptotic regulators rarely do (Díaz-Martínez et al., 2014). This suggests

that CAD-dependent DNA damage incurred during mitosis activates p53 following slippage (Orth et al., 2012). In addition to being an inhibitor of CAD, ICAD is also a chaperone essential for CAD function (Nagase et al., 2003), and accordingly, inhibition of both ICAD and Myc reduced CAD (Figure S7A). Moreover, ICAD RNAi suppressed DiM (Figure 8A), suggesting that by stabilizing CAD, Myc promotes accumulation of DNA damage during mitosis thereby accelerating DiM. Consistently, γ -H2AX accumulation was less prevalent in taxol-treated Myc RNAi cells (Figure S7B).

We were also intrigued by the very rapid DiM in cells lacking Bcl-xL and Mcl1 (Figure S3F). In addition, we noticed that in the absence of taxol, Bcl-xL/Mcl1-deficient cells often died upon mitotic entry (Figure S7C). However, it seems unlikely that ICAD/CAD-dependent damage accumulates fast enough to trigger apoptosis during an unperturbed mitosis. Indeed, ICAD RNAi had little protective effect in cells co-depleted for

that the two networks governing mitotic fate are rather different: while the SAC consists of essential genes, the DiM network involves redundant sub-networks. Myc drives expression of the apoptotic network required for DiM, providing a simple explanation for why it manifested in the screen. The different architectures of the two networks may reflect evolutionary origins and/or buffering capacities. The SAC, which is conserved from yeast to man, is an “all-or-nothing” mechanism that responds to a single input, unattached kinetochores, and is not buffered by transcription (Lara-Gonzalez et al., 2012). In contrast, apoptosis, a metazoan characteristic, responds to multiple inputs and can be “fine-tuned” by transcriptional buffering depending on developmental context and homeostatic pressures (Barkett and Gilmore, 1999). The differing architectures also support the notion that they are largely independent (Gascoigne and Taylor, 2008; Huang et al., 2010).

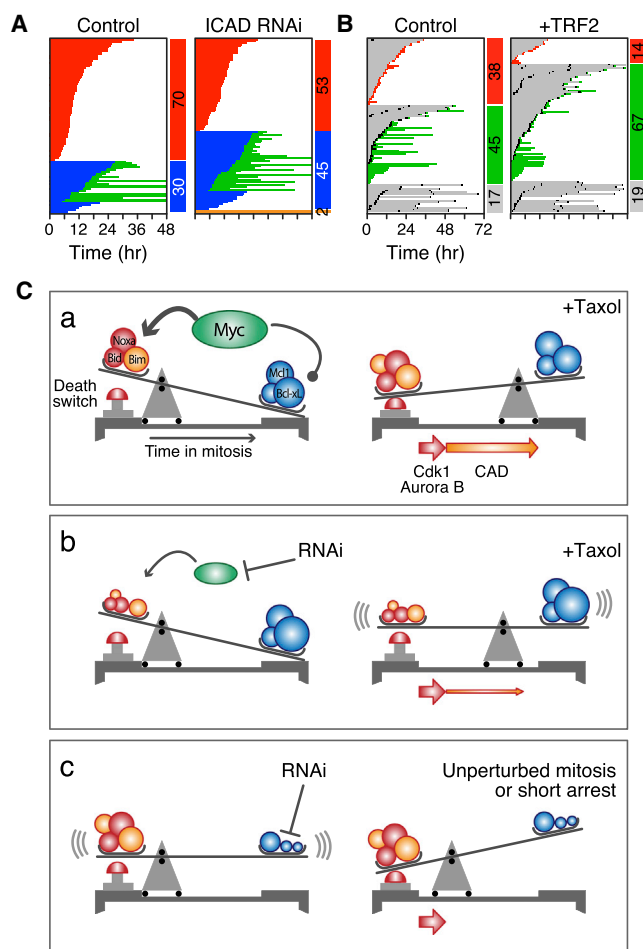


Figure 8. Inhibition of ICAD Enhances Slippage

(A) Fate profiles of RKO cells exposed to 0.1 μ M taxol following ICAD RNAi. (B) Fate profiles of RKO cells in the absence of taxol following RNAi-mediated co-repression Bcl-xL/Mcl1 plus tet-induced overexpression of TRF2. In (B), 0 hr represents when imaging started. (C) Mechanistic model, see text for details. See also Figure S7.

In addition to driving proliferation, Myc overexpression drives apoptosis via ARF-MDM2-p53 (McMahon, 2014). Because p53 is disengaged during mitosis, it is not clear how this mechanism could contribute to DiM, and indeed p53 is not required for Myc-dependent mitotic death. Moreover, Myc can upregulate Bim, Bid, and Noxa independently of p53 (Campone et al., 2011; Egle et al., 2004; Eischen et al., 2001; Hemann et al., 2005; Iacchino et al., 2003; Muthalagu et al., 2014; Nikiforov et al., 2007). Recent evidence shows that Myc drives p53-independent apoptosis by cooperating with Egr1, itself a Myc target (Boone et al., 2011). Myc promotes *EGR1* expression via a non-canonical mechanism involving ARF and in turn, Myc and Egr1 are co-recruited to the promoters of *BIM* and *NOXA* (Boone et al., 2011; Wirth et al., 2014). It seems likely, therefore, that in interphase, Myc and Egr1 upregulate a cluster of redundant pro-apoptotic BH3-only proteins and suppress Bcl-xL, establishing the apoptotic network which can later induce DiM without the need for p53 engagement and de novo gene expression. Upon

entry into mitosis, the apoptotic network is balanced so that a pro-survival environment is maintained (Figure 8C). However, in the presence of mitotic blockers, the balance slowly tips in favor of the pro-apoptotic BH3-only proteins, eventually triggering cell death. Several processes help tip the balance, including accumulation of DNA damage due to partial CAD activation and telomere deprotection (Hayashi et al., 2012; Orth et al., 2012). Also, slow degradation of Mcl1, possibly due to incomplete APC/C inhibition (Harley et al., 2010), weakens pro-survival function. When Myc is inhibited, the initial balance is more heavily weighted toward pro-survival, mitotic death is thus delayed providing more time for CyclinB1 degradation and slippage. Myc inhibition may also suppress DNA damage accumulation, weakening the apoptotic trigger. When Bcl-xL and Mcl1 are co-inhibited, the balance is so heavily weighted toward pro-death that cells cannot survive a short mitotic arrest, and even an unperturbed mitosis can induce apoptosis.

Myc is also required for efficient apoptosis in response to drugs that drive cells through an aberrant mitosis. Whether this is because these cells inherit an apoptotic balance tipped in favor of pro-survival or cannot initiate a robust post-mitotic response remains to be seen. Consistent with the latter, Myc also promotes cell cycle restraint following SAC override. One possibility to account for this is the ARF-MDM2-p53 pathway; by inducing ARF and thus suppressing MDM2, Myc may sensitize the p53-dependent mechanism that detects DNA damage incurred when chromosomes missegregate (Janssen et al., 2011). This may explain why ARF-deficient mouse embryonic fibroblasts tolerate aneuploidies (Silk et al., 2013). Alternatively, following chromosome missegregation induced by SAC override, Myc's ability to drive global gene expression might elevate the proteotoxic burden that arises in aneuploid daughter cells, thus enhancing cell cycle suppression (Tang and Amon, 2013). Interestingly, several mitotic regulators are synthetic lethal with Myc overexpression, including Cdk1, Survivin, Aurora B, and the SUMO-activating enzyme SAE-2 (den Hollander et al., 2010; Goga et al., 2007; Kessler et al., 2012; Yang et al., 2010). Whether this is due to deregulation of mitosis per se as opposed to deregulation of cellular responses to mitotic abnormalities is unclear. Consistent with the former, SAE-2 modulates a spindle assembly gene expression program (Kessler et al., 2012). Consistent with the latter, our observations show that Myc enhances both DiM and post-mitotic responses.

Antimitotic agents continue to be important frontline drugs, emphasized by the impressive effect of combining taxanes with targeted therapies in the treatment of breast cancer (Slamon et al., 2001). Whether taxanes inhibit tumor growth via antimitotic or other tubulin-dependent mechanisms remains unclear (Komlodi-Pasztor et al., 2012; Mitchison, 2012). Consistent with Myc enhancing antimitotic apoptosis, ovarian cancers treated with taxol and carboplatin responded better if Myc was more highly expressed (Iba et al., 2004). Consistently, Her2-negative breast cancers that responded to docetaxel and capecitabine had higher Myc levels. The correlation between Myc and cell cycle/SAC genes is especially striking because Her2-positive tumors do not show a similar pattern. This suggests that docetaxel-capecitabine responses require cell cycle progression and a robust SAC response. In contrast, anti-tumor effects mediated by trastuzumab-docetaxel-capecitabine are more likely dominated by

inhibition of Her2-dependent PI3K/Akt survival signaling (Berns et al., 2007), and therefore less dependent on mitotic entry and SAC activation. Taken together, these observations suggest that the Myc network may yield potential biomarkers. However, a recent study found that while triple-negative breast cancers exhibited elevated Myc expression, this did not predict responses to neoadjuvant chemotherapy (Horiuchi et al., 2012). Consistent with the mechanisms we describe here, this study did however observe that elevated Myc sensitized triple-negative cells to Cdk1 inhibition in a Bim-dependent, p53-independent manner. Thus, taking together our observations, the synthetic lethality relationships described above, and the provocative clinical observations, there is considerable merit in further exploring the links between the BH3-only/Bcl-xL pathway and mitotic regulators in the context of Myc-driven tumors. Interestingly, Myc inhibition had little effect on three cell lines we studied, suggesting that this avenue may provide insight into intrinsic resistance, while changes and/or heterogeneity in Myc expression may provide insight into acquired taxane resistance.

Myc suppresses Bcl-xL in various contexts (Eischen et al., 2001) and they inversely correlate in the breast cancer gene expression profiles we analyzed. Moreover, Bcl-xL overexpression potently blocks Myc-driven apoptosis (Pelengaris et al., 2002) and our observations reaffirm Bcl-xL as a potent mitotic survival factor. Although Mcl1 and Bcl-xL can partially compensate for each other during mitosis (Shi et al., 2011), degradation of Mcl1 during a mitotic arrest means that Bcl-xL becomes particularly critical following slippage. Because slippage is a clinically relevant phenotype (Zasadil et al., 2014), these observations make a compelling case for combining Bcl-xL inhibitors with antimetabolic agents. Indeed, the Bcl2/Bcl-xL inhibitor navitoclax sensitizes ovarian cancer cell lines to taxol (Wong et al., 2012). Similar combination strategies may also help revive the prospects of targeted antimetabolic agents that have thus far been disappointing in the clinic (Komlodi-Pasztor et al., 2012; Mitchison, 2012). Exploring Myc-dependent apoptotic pathways for predictive biomarkers may also facilitate better clinical evaluation of these agents. Finally, as a potent driver of tumorigenesis, Myc is itself an attractive anti-cancer target (McKeown and Bradner, 2014; Sodir and Evan, 2011). However, if superimposed on existing taxane chemotherapy regimens, targeting Myc may be counterproductive, weakening both the SAC and post-mitotic apoptosis, thereby fueling genomic instability. This should not detract from Myc as a target as long as mitigating strategies are also explored. Our observation that pharmacological inhibition of Bcl-xL potently restores apoptosis in Myc-deficient cells exposed to low-dose taxol further supports the case for exploring Bcl-xL inhibitors in the context of antimetabolic agents.

EXPERIMENTAL PROCEDURES

siRNA Library Screen

RKO cells were synchronized for 16 hr using 2 mM thymidine, released then seeded in 96-well plates (Greiner Bio-One) containing Opti-MEM media (Life Technologies), DharmaFECT 1 transfection reagent (Dharmacon), and siRNAs at a final concentration of 66 nM, after which 0.1 μ M taxol and viability reagent (CellTiter 96 AQueousOne Solution Cell Proliferation Assay, Promega) were added after 24 and 68 hr, respectively, and the absorbance at 490 nm measured after 72 hr. For the tertiary screen, the mitotic index at 24 hr was

determined using a BD Pathway (BD Biosciences). Cell lines and small molecule inhibitors are described in the [Supplemental Experimental Procedures](#).

Functional Experiments

siRNAs and DharmaFECT 1 combined in Opti-MEM media were added to RKO cells plated at 10×10^4 cells/ml, yielding a final siRNA concentration of 66 nM. For siRNA sequences, see the [Supplemental Experimental Procedures](#). Open reading frames described in the [Supplemental Experimental Procedures](#) were cloned into pcDNA5/FRT/TO based vectors and isogenic, tetracycline-inducible, stable cell lines generated by co-transfection with pOG44 (Invitrogen) into Flp-In T-REx RKO cells. Phase contrast imaging, cell proliferation, and apoptosis measurements were performed on an IncuCyte ZOOM (EssenBioScience) with CellPlayer Kinetic Caspase-3/7 Apoptosis Assay Kit (EssenBioSciences). Image sequences were analyzed manually and statistical analysis performed with GraphPad Prism. On fate profiles, 0 hr corresponds to mitotic entry unless stated otherwise in the legend. Immunoblotting was performed using antibodies described in the [Supplemental Experimental Procedures](#).

Gene Expression Profiling

Cells transfected with siRNAs were synchronized, released for 5 hr, then RNA was prepared using Trizol (Life Technologies). One hundred nanograms of RNA was hybridized with custom nCounter Reporter and Capture probe sets (Nanostring Technologies) at 65°C overnight, unhybridized probes removed, complexes bound to the imaging surface, and images acquired using the nCounter Digital Analyzer. Transcript counts were normalized to housekeeping genes using nSolver Analysis Software. For global gene expression profiling, total RNA was processed using the Illumina TruSeq Stranded mRNA Sample Preparation Kit, then cDNA libraries sequenced on an Illumina HiSeq 2000 using single read, 50 cycle runs. Quality of sequencing reads was assessed using FastQC (Babraham Bioinformatics) and aligned to a reference genome (hg19, UCSC Genome Browser) using TopHat. Sequencing yielded on average 23.7 million unique reads per sample with a 60.7%–65.7% mapping rate. Cufflinks was used to generate transcript abundance as fragments per kilobase of transcript per million mapped reads (FPKM), and statistical analysis of FPKM values was calculated using R (Bioconductor).

Inactivation of Myc in the Mouse Intestine

Cre-mediated inactivation of *MYC* in the intestinal epithelium was induced via three intraperitoneal (i.p.) injections of 80 mg/kg β -naphthoflavone in 1 day. Four days later, 10 mg/kg taxol was administered via i.p. injection, tissue harvested after various time points, fixed in 4% formaldehyde, then stained for cleaved caspase 3 (R&D systems). All animal experiments were conducted under an appropriate animal project license approved by the UK home office and in accordance with the Animal Welfare and Experimental Ethics Committee at the University of Glasgow.

Statistical Methods

Statistical analysis was performed in GraphPad Prism 6 as follows: ANOVA plus Bonferroni (Figures 2C and 2F); linear regression (Figure 2D); correlation (Figures S1B and 5E); Paired t test (Figure 2G); Wilcoxon t test (Figure 4A); Mann-Whitney (Figures 4B, 5A, 5B, 5D, 6, S3A, S3I, and S5B); Kruskal-Wallis (Figure S1E). In figures, p values were *p < 0.05, **p < 0.01, ***p < 0.001, ****p < 0.0001. Scatterplots show mean and SD. Unless stated otherwise in the figure legend, box-and-whisker plots show median, interquartile ranges, plus min to max range. Figure S1D, mean \pm SD; Figure S4B, mean \pm SEM.

ACCESSION NUMBERS

The accession number for the global gene expression data reported in this paper is GEO: GSE68219.

SUPPLEMENTAL INFORMATION

Supplemental Information includes Supplemental Experimental Procedures, seven figures, and seven tables and can be found with this article online at <http://dx.doi.org/10.1016/j.ccell.2015.06.001>.

AUTHOR CONTRIBUTIONS

C.T. performed the RNAi screen, Nanostring analysis, and functional experiments. A.T., A.B., O.S., L.N., S.L., and C.S. contributed to the functional experiments. R.A.R., D.H., and O.J.S. contributed the mouse data. B.B. and D.J.P. synthesized the Cenp-E inhibitor. P.L., Y.S., and D.W.C. contributed the HiSeq analysis. S.S.T. conceived the study and wrote the manuscript. All authors read and commented on the manuscript.

ACKNOWLEDGMENTS

This work was supported by the Genomic Technologies and Bioimaging Core Facilities in the Faculty of Life Sciences. We thank Stefan Knapp (University of Oxford) and Bert Vogelstein (Johns Hopkins) for reagents; and Andy Hayes, Leo Zeef, Dave Spiller, Andy Sharrocks, Mike White, Gino Poulin, Donald Ogilvie, Dean Jackson, and William Weiss for useful discussions. Funding was provided by Cancer Research UK, the Medical Research Council, and the Wellcome Trust. S.S.T. is supported by a Cancer Research UK Senior Fellowship.

Received: October 10, 2014

Revised: March 4, 2015

Accepted: June 8, 2015

Published: July 13, 2015

REFERENCES

- A'Hern, R.P., Jamal-Hanjani, M., Szász, A.M., Johnston, S.R., Reis-Filho, J.S., Roylance, R., and Swanton, C. (2013). Taxane benefit in breast cancer—a role for grade and chromosomal stability. *Nat. Rev. Clin. Oncol.* *10*, 357–364.
- Bah, N., Maillet, L., Ryan, J., Dubreil, S., Gautier, F., Letai, A., Juin, P., and Barillé-Nion, S. (2014). Bcl-xL controls a switch between cell death modes during mitotic arrest. *Cell Death Dis.* *5*, e1291.
- Barkett, M., and Gilmore, T.D. (1999). Control of apoptosis by Rel/NF-kappaB transcription factors. *Oncogene* *18*, 6910–6924.
- Berns, K., Horlings, H.M., Hennessy, B.T., Madiredjo, M., Hijmans, E.M., Beelen, K., Linn, S.C., Gonzalez-Angulo, A.M., Stemke-Hale, K., Hauptmann, M., et al. (2007). A functional genetic approach identifies the PI3K pathway as a major determinant of trastuzumab resistance in breast cancer. *Cancer Cell* *12*, 395–402.
- Boone, D.N., Qi, Y., Li, Z., and Hann, S.R. (2011). Egr1 mediates p53-independent c-Myc-induced apoptosis via a noncanonical ARF-dependent transcriptional mechanism. *Proc. Natl. Acad. Sci. USA* *108*, 632–637.
- Brito, D.A., and Rieder, C.L. (2006). Mitotic checkpoint slippage in humans occurs via cyclin B destruction in the presence of an active checkpoint. *Curr. Biol.* *16*, 1194–1200.
- Campone, M., Noël, B., Couriaud, C., Grau, M., Guillemin, Y., Gautier, F., Gouraud, W., Charbonnel, C., Campion, L., Jézéquel, P., et al. (2011). c-Myc dependent expression of pro-apoptotic Bim renders HER2-overexpressing breast cancer cells dependent on anti-apoptotic Mcl-1. *Mol. Cancer* *10*, 110.
- Conacci-Sorrell, M., McFerrin, L., and Eisenman, R.N. (2014). An overview of MYC and its interactome. *Cold Spring Harb Perspect Med* *4*, a014357.
- den Hollander, J., Rimpí, S., Doherty, J.R., Rudelius, M., Buck, A., Hoellein, A., Kremer, M., Graf, N., Scheerer, M., Hall, M.A., et al. (2010). Aurora kinases A and B are up-regulated by Myc and are essential for maintenance of the malignant state. *Blood* *116*, 1498–1505.
- Díaz-Martínez, L.A., Karamysheva, Z.N., Warrington, R., Li, B., Wei, S., Xie, X.J., Roth, M.G., and Yu, H. (2014). Genome-wide siRNA screen reveals coupling between mitotic apoptosis and adaptation. *EMBO J.* *33*, 1960–1976.
- Dumontet, C., and Jordan, M.A. (2010). Microtubule-binding agents: a dynamic field of cancer therapeutics. *Nat. Rev. Drug Discov.* *9*, 790–803.
- Egle, A., Harris, A.W., Bouillet, P., and Cory, S. (2004). Bim is a suppressor of Myc-induced mouse B cell leukemia. *Proc. Natl. Acad. Sci. USA* *101*, 6164–6169.
- Eichhorn, J.M., Alford, S.E., Sakurikar, N., and Chambers, T.C. (2014). Molecular analysis of functional redundancy among anti-apoptotic Bcl-2 proteins and its role in cancer cell survival. *Exp. Cell Res.* *322*, 415–424.
- Eick, D., and Bornkamm, G.W. (1986). Transcriptional arrest within the first exon is a fast control mechanism in c-myc gene expression. *Nucleic Acids Res.* *14*, 8331–8346.
- Eilers, M., and Eisenman, R.N. (2008). Myc's broad reach. *Genes Dev.* *22*, 2755–2766.
- Eischen, C.M., Woo, D., Roussel, M.F., and Cleveland, J.L. (2001). Apoptosis triggered by Myc-induced suppression of Bcl-X(L) or Bcl-2 is bypassed during lymphomagenesis. *Mol. Cell. Biol.* *21*, 5063–5070.
- Filippakopoulos, P., Qi, J., Picaud, S., Shen, Y., Smith, W.B., Fedorov, O., Morse, E.M., Keates, T., Hickman, T.T., Felletar, I., et al. (2010). Selective inhibition of BET bromodomains. *Nature* *468*, 1067–1073.
- Garnett, M.J., Edelman, E.J., Heidorn, S.J., Greenman, C.D., Dastur, A., Lau, K.W., Greninger, P., Thompson, I.R., Luo, X., Soares, J., et al. (2012). Systematic identification of genomic markers of drug sensitivity in cancer cells. *Nature* *483*, 570–575.
- Gascoigne, K.E., and Taylor, S.S. (2008). Cancer cells display profound intra- and interline variation following prolonged exposure to antimetabolic drugs. *Cancer Cell* *14*, 111–122.
- Gascoigne, K.E., and Taylor, S.S. (2009). How do anti-mitotic drugs kill cancer cells? *J. Cell Sci.* *122*, 2579–2585.
- Glück, S., Ross, J.S., Royce, M., McKenna, E.F., Jr., Perou, C.M., Avisar, E., and Wu, L. (2012). TP53 genomics predict higher clinical and pathologic tumor response in operable early-stage breast cancer treated with docetaxel-cyclophosphamide ± trastuzumab. *Breast Cancer Res. Treat.* *132*, 781–791.
- Goga, A., Yang, D., Tward, A.D., Morgan, D.O., and Bishop, J.M. (2007). Inhibition of CDK1 as a potential therapy for tumors over-expressing MYC. *Nat. Med.* *13*, 820–827.
- Hann, S.R. (2014). MYC cofactors: molecular switches controlling diverse biological outcomes. *Cold Spring Harb Perspect Med* *4*, a014399.
- Harley, M.E., Allan, L.A., Sanderson, H.S., and Clarke, P.R. (2010). Phosphorylation of Mcl-1 by CDK1-cyclin B1 initiates its Cdc20-dependent destruction during mitotic arrest. *EMBO J.* *29*, 2407–2420.
- Hayashi, M.T., Cesare, A.J., Fitzpatrick, J.A.J., Lazzarini-Denchi, E., and Karlseder, J. (2012). A telomere-dependent DNA damage checkpoint induced by prolonged mitotic arrest. *Nat. Struct. Mol. Biol.* *19*, 387–394.
- Hemann, M.T., Bric, A., Teruya-Feldstein, J., Herbst, A., Nilsson, J.A., Cordon-Cardo, C., Cleveland, J.L., Tansey, W.P., and Lowe, S.W. (2005). Evasion of the p53 tumour surveillance network by tumour-derived MYC mutants. *Nature* *436*, 807–811.
- Horiuchi, D., Kusdra, L., Huskey, N.E., Chandriani, S., Lenburg, M.E., Gonzalez-Angulo, A.M., Creasman, K.J., Bazarov, A.V., Smyth, J.W., Davis, S.E., et al. (2012). MYC pathway activation in triple-negative breast cancer is synthetic lethal with CDK inhibition. *J. Exp. Med.* *209*, 679–696.
- Huang, H.C., Mitchison, T.J., and Shi, J. (2010). Stochastic competition between mechanistically independent slippage and death pathways determines cell fate during mitotic arrest. *PLoS ONE* *5*, e15724.
- laccarino, I., Hancock, D., Evan, G., and Downward, J. (2003). c-Myc induces cytochrome c release in Rat1 fibroblasts by increasing outer mitochondrial membrane permeability in a Bid-dependent manner. *Cell Death Differ.* *10*, 599–608.
- Iba, T., Kigawa, J., Kanamori, Y., Itamochi, H., Oishi, T., Simada, M., Uegaki, K., Naniwa, J., and Terakawa, N. (2004). Expression of the c-myc gene as a predictor of chemotherapy response and a prognostic factor in patients with ovarian cancer. *Cancer Sci.* *95*, 418–423.
- Janssen, A., van der Burg, M., Szuhai, K., Kops, G.J., and Medema, R.H. (2011). Chromosome segregation errors as a cause of DNA damage and structural chromosome aberrations. *Science* *333*, 1895–1898.
- Keen, N., and Taylor, S. (2009). Mitotic drivers—inhibitors of the Aurora B Kinase. *Cancer Metastasis Rev.* *28*, 185–195.
- Kessler, J.D., Kahle, K.T., Sun, T., Meerbrey, K.L., Schlabach, M.R., Schmitt, E.M., Skinner, S.O., Xu, Q., Li, M.Z., Hartman, Z.C., et al. (2012). A

- SUMOylation-dependent transcriptional subprogram is required for Myc-driven tumorigenesis. *Science* 335, 348–353.
- Komlodi-Pasztor, E., Sackett, D.L., and Fojo, A.T. (2012). Inhibitors targeting mitosis: tales of how great drugs against a promising target were brought down by a flawed rationale. *Clin. Cancer Res.* 18, 51–63.
- Lara-Gonzalez, P., Westhorpe, F.G., and Taylor, S.S. (2012). The spindle assembly checkpoint. *Curr. Biol.* 22, R966–R980.
- Lessene, G., Czabotar, P.E., Sleebs, B.E., Zobel, K., Lowes, K.N., Adams, J.M., Baell, J.B., Colman, P.M., Deshayes, K., Fairbrother, W.J., et al. (2013). Structure-guided design of a selective BCL-X(L) inhibitor. *Nat. Chem. Biol.* 9, 390–397.
- Li, Q., and Dang, C.V. (1999). c-Myc overexpression uncouples DNA replication from mitosis. *Mol. Cell. Biol.* 19, 5339–5351.
- Lowe, S.W., Cepero, E., and Evan, G. (2004). Intrinsic tumour suppression. *Nature* 432, 307–315.
- McKeown, M.R., and Bradner, J.E. (2014). Therapeutic strategies to inhibit MYC. *Cold Spring Harb Perspect Med* 4, a014266.
- McMahon, S.B. (2014). MYC and the control of apoptosis. *Cold Spring Harb Perspect Med* 4, a014407.
- Minn, A.J., Boise, L.H., and Thompson, C.B. (1996). Expression of Bcl-xL and loss of p53 can cooperate to overcome a cell cycle checkpoint induced by mitotic spindle damage. *Genes Dev.* 10, 2621–2631.
- Mitchison, T.J. (2012). The proliferation rate paradox in antimetabolic chemotherapy. *Mol. Biol. Cell* 23, 1–6.
- Murray, S., Briasoulis, E., Linardou, H., Bafaloukos, D., and Papadimitriou, C. (2012). Taxane resistance in breast cancer: mechanisms, predictive biomarkers and circumvention strategies. *Cancer Treat. Rev.* 38, 890–903.
- Muthalagu, N., Junttila, M.R., Wiese, K.E., Wolf, E., Morton, J., Bauer, B., Evan, G.I., Eilers, M., and Murphy, D.J. (2014). BIM is the primary mediator of MYC-induced apoptosis in multiple solid tissues. *Cell Rep.* 8, 1347–1353.
- Nagase, H., Fukuyama, H., Tanaka, M., Kawane, K., and Nagata, S. (2003). Mutually regulated expression of caspase-activated DNase and its inhibitor for apoptotic DNA fragmentation. *Cell Death Differ.* 10, 142–143.
- Nikiforov, M.A., Riblett, M., Tang, W.H., Gratchouk, V., Zhuang, D., Fernandez, Y., Verhaegen, M., Varambally, S., Chinnaiyan, A.M., Jakubowiak, A.J., and Soengas, M.S. (2007). Tumor cell-selective regulation of NOXA by c-MYC in response to proteasome inhibition. *Proc. Natl. Acad. Sci. USA* 104, 19488–19493.
- Orth, J.D., Loewer, A., Lahav, G., and Mitchison, T.J. (2012). Prolonged mitotic arrest triggers partial activation of apoptosis, resulting in DNA damage and p53 induction. *Mol. Biol. Cell* 23, 567–576.
- Pelengaris, S., Khan, M., and Evan, G.I. (2002). Suppression of Myc-induced apoptosis in beta cells exposes multiple oncogenic properties of Myc and triggers carcinogenic progression. *Cell* 109, 321–334.
- Pheesse, T.J., Myant, K.B., Cole, A.M., Ridgway, R.A., Pearson, H., Muncan, V., van den Brink, G.R., Vousden, K.H., Sears, R., Vassilev, L.T., et al. (2014). Endogenous c-Myc is essential for p53-induced apoptosis in response to DNA damage in vivo. *Cell Death Differ.* 21, 956–966.
- Radulescu, S., Ridgway, R.A., Appleton, P., Kroboth, K., Patel, S., Woodgett, J., Taylor, S., Nathke, I.S., and Sansom, O.J. (2010). Defining the role of APC in the mitotic spindle checkpoint in vivo: APC-deficient cells are resistant to Taxol. *Oncogene* 29, 6418–6427.
- Rieder, C.L., and Maiato, H. (2004). Stuck in division or passing through: what happens when cells cannot satisfy the spindle assembly checkpoint. *Dev. Cell* 7, 637–651.
- Shi, J., Zhou, Y., Huang, H.C., and Mitchison, T.J. (2011). Navitoclax (ABT-263) accelerates apoptosis during drug-induced mitotic arrest by antagonizing Bcl-xL. *Cancer Res.* 71, 4518–4526.
- Silk, A.D., Zasadil, L.M., Holland, A.J., Vitre, B., Cleveland, D.W., and Weaver, B.A. (2013). Chromosome missegregation rate predicts whether aneuploidy will promote or suppress tumors. *Proc. Natl. Acad. Sci. USA* 110, E4134–E4141.
- Slamon, D.J., Leyland-Jones, B., Shak, S., Fuchs, H., Paton, V., Bajamonde, A., Fleming, T., Eiermann, W., Wolter, J., Pegram, M., et al. (2001). Use of chemotherapy plus a monoclonal antibody against HER2 for metastatic breast cancer that overexpresses HER2. *N. Engl. J. Med.* 344, 783–792.
- Sodir, N.M., and Evan, G.I. (2011). Finding cancer's weakest link. *Oncotarget* 2, 1307–1313.
- Soucek, L., Jucker, R., Panacchia, L., Ricordy, R., Tatò, F., and Nasi, S. (2002). Omomyc, a potential Myc dominant negative, enhances Myc-induced apoptosis. *Cancer Res.* 62, 3507–3510.
- Tang, Y.C., and Amon, A. (2013). Gene copy-number alterations: a cost-benefit analysis. *Cell* 152, 394–405.
- Taylor, S.S., and McKeon, F. (1997). Kinetochore localization of murine Bub1 is required for normal mitotic timing and checkpoint response to spindle damage. *Cell* 89, 727–735.
- Thompson, S.L., and Compton, D.A. (2010). Proliferation of aneuploid human cells is limited by a p53-dependent mechanism. *J. Cell Biol.* 188, 369–381.
- Topham, C.H., and Taylor, S.S. (2013). Mitosis and apoptosis: how is the balance set? *Curr. Opin. Cell Biol.* 25, 780–785.
- Upreti, M., Galitovskaya, E.N., Chu, R., Tackett, A.J., Terrano, D.T., Granell, S., and Chambers, T.C. (2008). Identification of the major phosphorylation site in Bcl-xL induced by microtubule inhibitors and analysis of its functional significance. *J. Biol. Chem.* 283, 35517–35525.
- Weaver, B.A. (2014). How Taxol/paclitaxel kills cancer cells. *Mol. Biol. Cell* 25, 2677–2681.
- Wiese, K.E., Walz, S., von Eyss, B., Wolf, E., Athineos, D., Sansom, O., and Eilers, M. (2013). The role of MIZ-1 in MYC-dependent tumorigenesis. *Cold Spring Harb Perspect Med* 3, a014290.
- Wirth, M., Stojanovic, N., Christian, J., Paul, M.C., Stauber, R.H., Schmid, R.M., Häcker, G., Krämer, O.H., Saur, D., and Schneider, G. (2014). MYC and EGR1 synergize to trigger tumor cell death by controlling NOXA and BIM transcription upon treatment with the proteasome inhibitor bortezomib. *Nucleic Acids Res.* 42, 10433–10447.
- Wolf, E., Lin, C.Y., Eilers, M., and Levens, D.L. (2015). Taming of the beast: shaping Myc-dependent amplification. *Trends Cell Biol.* 25, 241–248.
- Wong, M., Tan, N., Zha, J., Peale, F.V., Yue, P., Fairbrother, W.J., and Belmont, L.D. (2012). Navitoclax (ABT-263) reduces Bcl-x(L)-mediated chemoresistance in ovarian cancer models. *Mol. Cancer Ther.* 11, 1026–1035.
- Yang, D., Liu, H., Goga, A., Kim, S., Yuneva, M., and Bishop, J.M. (2010). Therapeutic potential of a synthetic lethal interaction between the MYC proto-oncogene and inhibition of aurora-B kinase. *Proc. Natl. Acad. Sci. USA* 107, 13836–13841.
- Zasadil, L.M., Andersen, K.A., Yeum, D., Rocque, G.B., Wilke, L.G., Tevaarwerk, A.J., Raines, R.T., Burkard, M.E., and Weaver, B.A. (2014). Cytotoxicity of paclitaxel in breast cancer is due to chromosome missegregation on multipolar spindles. *Sci. Transl. Med.* 6, 229–243.

Cancer Cell, Volume 28

Supplemental Information

MYC Is a Major Determinant of Mitotic Cell Fate

Caroline Topham, Anthony Tighe, Peter Ly, Ailsa Bennett, Olivia Sloss, Louisa Nelson, Rachel A. Ridgway, David Huels, Samantha Littler, Claudia Schandl, Ying Sun, Beatrice Bechi, David J. Procter, Owen J. Sansom, Don W. Cleveland, and Stephen S. Taylor

Supplemental Data

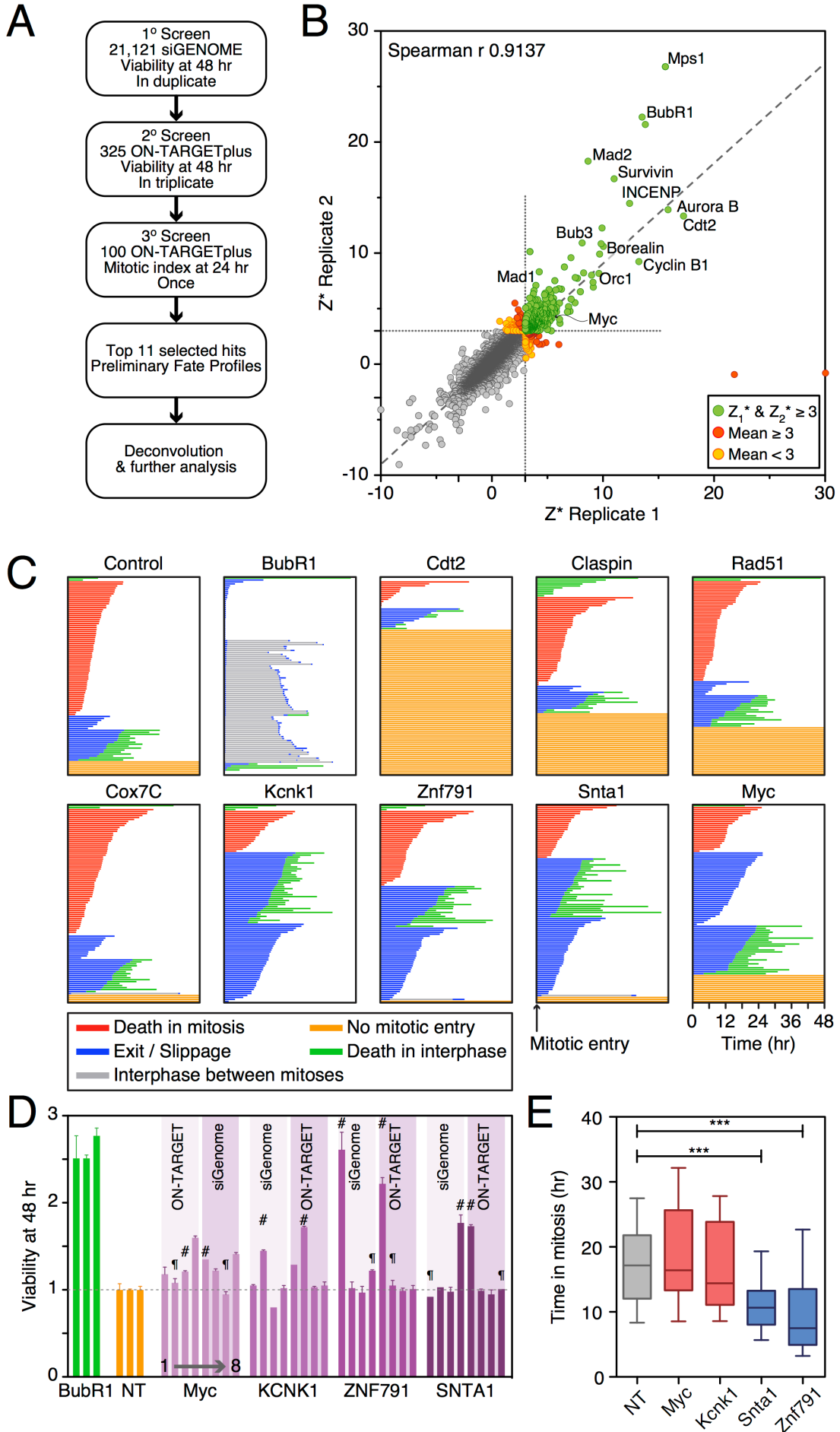


Figure S1, related to Figure 1. A genome-wide siRNA screen for regulators of mitotic cell fate. (A) Workflow of the screen. **(B)** Result of the primary screen, plotting the robust Z scores (Z^*) for the two replicates. Z^* scores were calculated using the median absolute deviation for each plate (Chung et al., 2008). Genes with mean Z^* scores greater than 3 were taken forward to the secondary screen. **(C)** Fate profiles of RKO cells transfected with selected ON-TARGETplus SMARTpools and exposed to 0.1 μ M taxol. **(D)** Bar graph showing viability of taxol-treated RKO cells after transfection of individual siRNAs from the SMARTpools used in the 1^o and 2^o screens. While siRNAs in many of the siGENOME and ON-TARGETplus SMARTpools are distinct, in some instances there is duplication, indicated by hashtags (#) and paragraph symbols (§). Myc siRNAs 4, 5, 6 and 8 repress Myc and inhibit death in mitosis (DiM) (Fig. S2A) so they were pooled and used for further experiments, while #4 was used in isolation for the RNAi-rescue experiment in Fig. S2B. Values represent mean and SD from two experiments. **(E)** Box-and-whisker plots (median, interquartile and 10-90% ranges) showing that in isolation, *SNTA1* #4 and *ZNF791* #1 accelerate mitotic exit. In contrast, the active *KCNKI* siRNA more closely resembles the Myc phenotype.

Table S1, related to Figure 1. Primary screen; MTS values at 48 hr. Used to generate Fig. S1B. (Provided as an Excel file).

Table S2, related to Figure 1. Secondary and tertiary screens; MTS values at 48 hr and mitotic index (granularity) values at 24 hr. Used to generate Fig. 1C. (Provided as an Excel file).

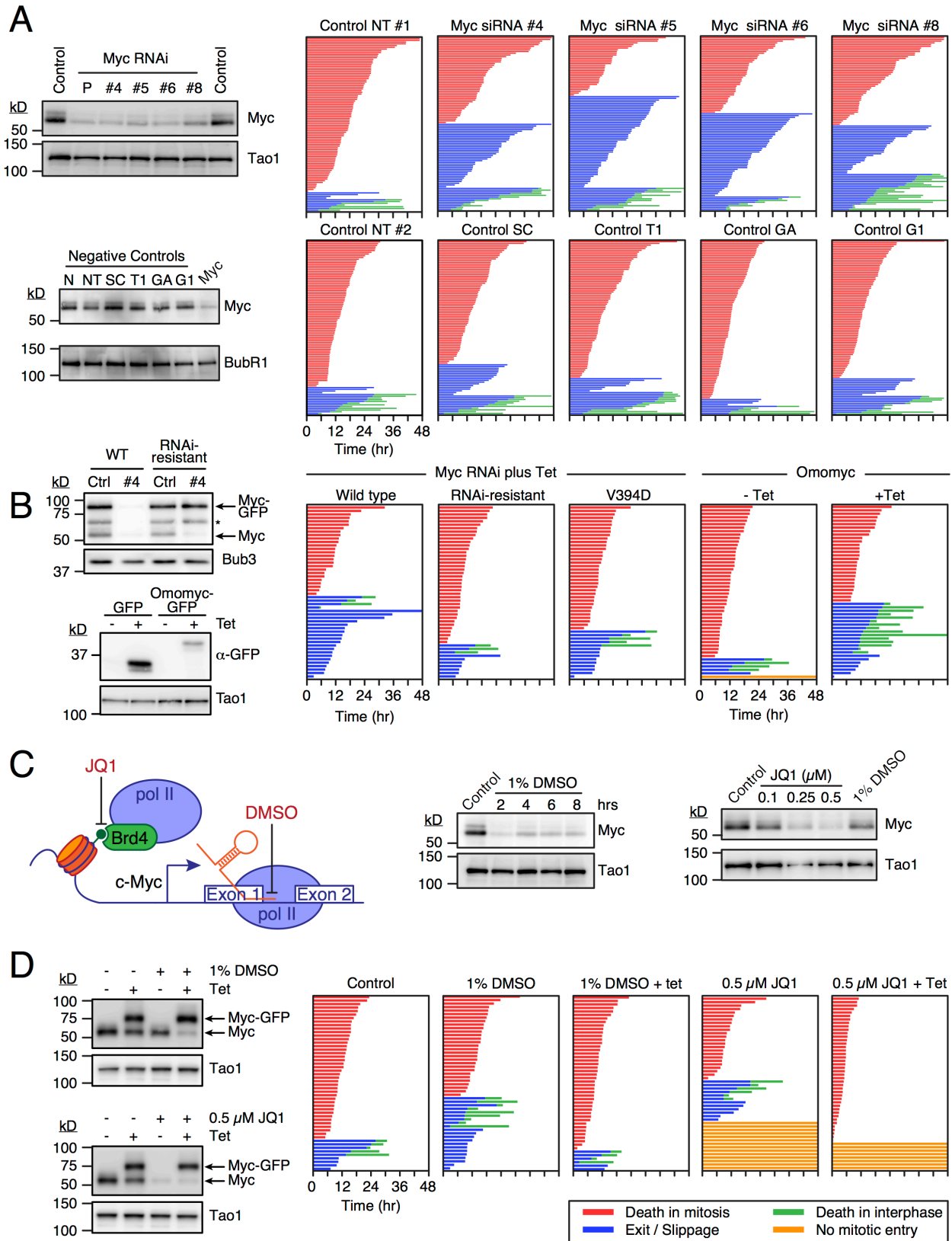


Figure S2, related to Figure 2. Myc is a regulator of mitotic cell fate. (A) Deconvolution of siRNA pools targeting Myc. Immunoblots of RKO cells transfected with four active Myc siRNAs, either as a pool (P) or individually (nos 4, 5, 6 and 8), and six negative controls siRNAs. Corresponding fate profiles of transfected RKO cells treated with 100nM taxol. (B) Analysis of Myc mutants. Immunoblots show induction of GFP-tagged Myc, an RNAi-resistant mutant and Omomyc in RKO cells treated with 1 μ g/ml tetracycline. The asterisk marks a Myc-GFP cleavage product. Fate profiles as in (A). (C) Schematic showing how DMSO and JQ1 inhibit transcription of *MYC* and immunoblots confirming that DMSO and JQ1 inhibit Myc in RKO cells. (D) Immunoblots and fate profiles showing that a Myc-GFP cDNA is resistant to DMSO and JQ1 and restores the balance back towards death in mitosis.

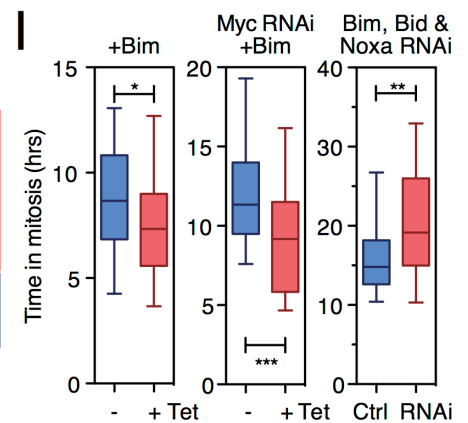
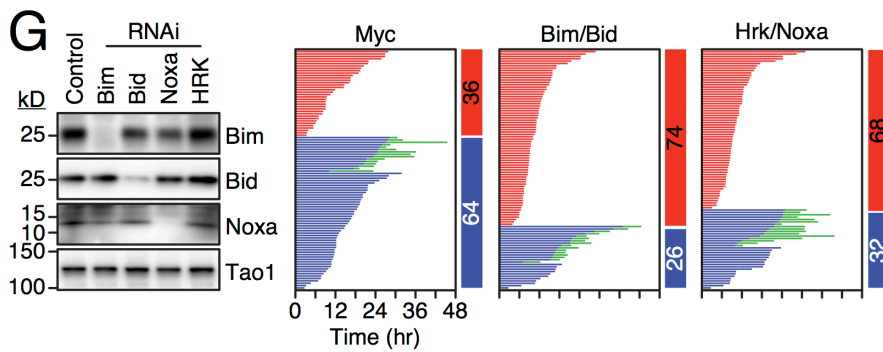
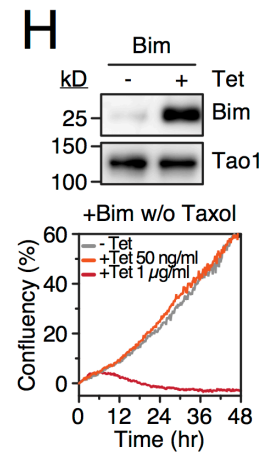
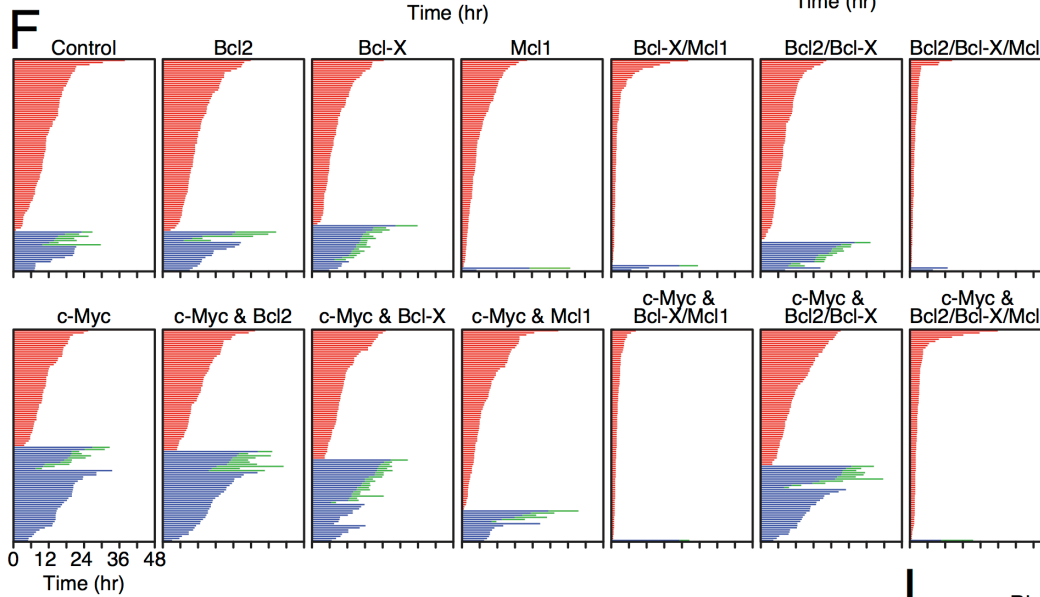
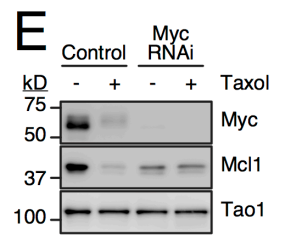
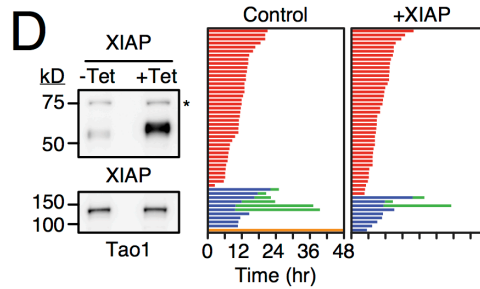
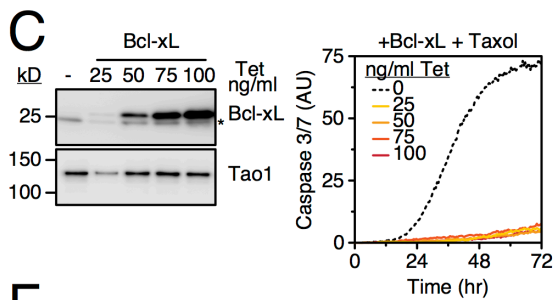
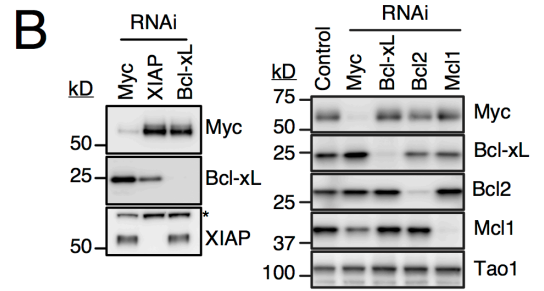
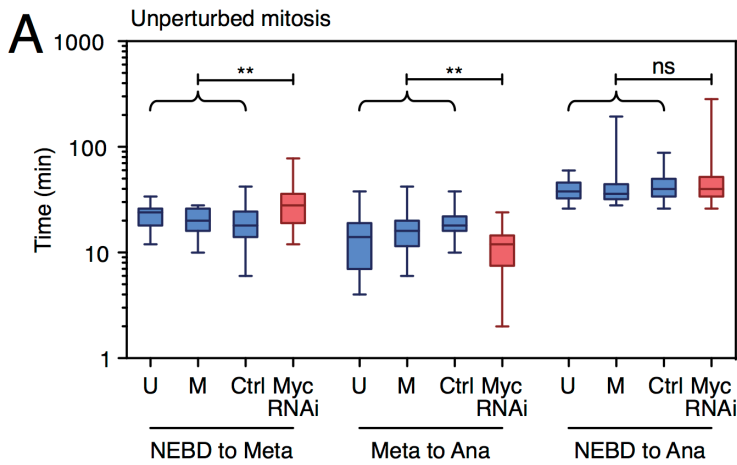


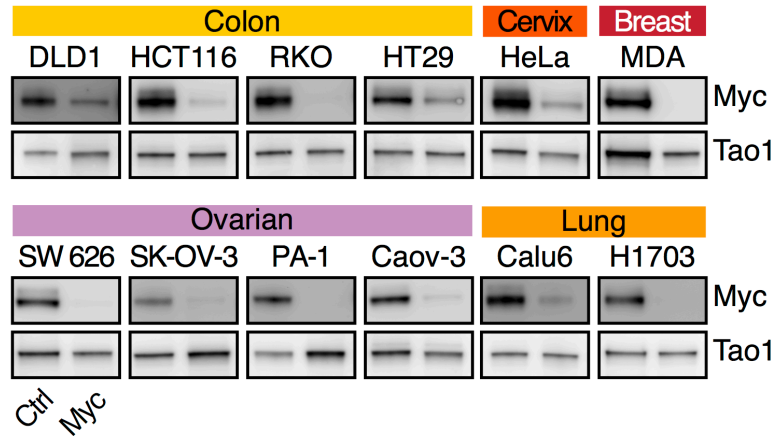
Figure S3, related to Figure 3. Analysis of Bcl2-family members. (A) Time lapse analysis of RKO cells expressing a GFP-tagged histone H2B, measuring the time from nuclear envelope breakdown (NEBD) to metaphase, from metaphase to anaphase and from NEBD to anaphase. Cells were either untreated (U), mock transfected (M), or transfected with siRNAs, either a non-targeting control (Ctrl) or the pool targeting Myc. Box-and-whisker plots show the median, interquartile ranges and full range. (B) Immunoblots showing RNAi-mediated inhibition of Myc, XIAP and pro-survival Bcl2 family proteins in RKO cells. Note that Myc RNAi results in up-regulation of Bcl-xL and down-regulation of Mcl1, but has no obvious effect on XIAP. Asterisk marks a non-specific background band. (C) Characterisation of a stable tet-inducible RKO cell line overexpressing Bcl-xL; immunoblot shows induction of Bcl-xL with a range of tetracycline concentrations. Asterisk marks the endogenous protein. Apoptosis assay shows that even low level induction of Bcl-xL is sufficient to block apoptosis induced by taxol. Note that 25ng/ml tetracycline increases Bcl-xL levels only two fold yet this is sufficient to block apoptosis. (D) Characterisation of a stable tet-inducible RKO cell line overexpressing XIAP; immunoblot shows induction of XIAP with 1 μ g/ml tetracycline. Asterisk marks a non-specific background band. Fate profile shows that tet-induced overexpression of XIAP does not inhibit DiM in 0.1 μ M taxol. (E) Immunoblot showing reduced Mcl1 levels in Myc RNAi cells. Consistent with Mcl1 being degraded in mitosis, Mcl1 is less abundant in taxol-treated cells. However, Mcl1 levels do not fall further in taxol-treated Myc RNAi cells, possibly due to inhibition of mitotic-specific degradation. (F) Fate profiles following RNAi-mediated inhibition of pro-survival Bcl2 family proteins showing that co-repression of Bcl-xL and Mcl1 leads to rapid DiM in 0.1 μ M taxol. (G) Immunoblots of RKO cells showing RNAi-mediated inhibition of the BH3-only proteins Bim, Bid and Noxa, and fate profiles showing that while Myc RNAi reduces DiM in 0.1 μ M taxol to 36% (compared to 69% in the corresponding control shown in Fig. 3D), repressing the BH3-only proteins, either in isolation (not shown) or in pairs as shown here, has little effect, with DiM remaining at ~70%. (H) Characterisation of an RKO tet-inducible cell line overexpressing Bim; immunoblot shows induction of Bim with 50 ng/ml tetracycline. The growth curves show that in the absence of taxol, overexpressing Bim to this level alone does not induce apoptosis. (I) Box-and-whisker plots (median, interquartile and 10-90 percentile range) showing the time spent arrested in mitosis following overexpression of Bim, either in control cells or following Myc RNAi, and following inhibition of Bim, Bid and Noxa. Note that overexpression of Bim accelerates death in mitosis while inhibition of the three BH3-only proteins delays death.

Table S3, related to Figure 3. Nanostring gene expression profiling data. Used to generate Fig. 3A.

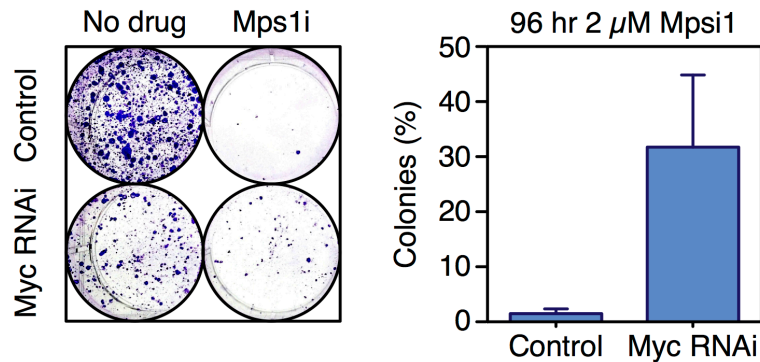
	Common name	Gene Name	Log2 fold change*	Reads		Common name	Gene Name	Log2 fold change*	Reads
Apoptosis module	AIF	AIFM1	-0.259	429	Mitosis module	Apc1	ANAPC1	-0.645	569
	Apaf1	APAF1	0.211	263		Apc10	ANAPC10	-0.253	193
	ATM	ATM	0.144	59		Cenp-S	APITD1	-0.602	285
	BAD	BAD	-0.039	69		Aurora A	AURKA	-0.552	1217
	BAK	Bak1	0.125	669		Aurora B	AURKB	-0.513	1315
	BAX	BAX	-0.042	756		Survivin	BIRC5	-0.720	927
	Bcl2	BCL2	-0.255	34		Bub1	BUB1	-0.435	1096
	Bcl-XL	BCL2L1	0.477	772		BubR1	BUB1B	-0.581	799
	BimEL	BCL2L11	-0.668	26		Kn11	CASC5	-0.204	498
	BID	BID	-0.912	187		Cyclin B1	CCNB1	-0.606	2911
	cIAP	BIRC3	-0.187	60		Cdc20	CDC20	-0.416	1731
	β-TrCP	BTRC	-0.180	194		Cdc25	CDC25A	-0.923	632
	Caspase 3	CASP3	0.318	359		Sororin	CDCA5	-0.540	895
	Caspase 7	CASP7	-0.242	261		Cdh1	CDK1	-0.514	2734
	Caspase 8	CASP8	-0.167	301		Cenp-E	CENPE	-0.332	542
	Casp8a	CASP8AP2	-0.276	191		Cenp-F	CENPF	-0.246	1208
	Caspase 9	CASP9	0.202	76		Cenp-T	CENPT	0.539	16
	c-FLIP	CFLAR	0.059	124		Separase	ESPL1	-0.231	337
	CKII	CSNK2B	-0.289	2061		Haspin	GSG2	-0.441	396
	ICAD	DFFA	-0.753	429		Augmin	HAUS1	-0.447	533
	SMAC	DIABLO	-0.242	193		Eg5	KIF11	-0.519	695
	E2F1	E2F1	-0.843	316		Mad2	MAD2L1	-0.762	1663
	Fadd	FADD	0.176	30		p31 comet	MAD2L1BP	-0.291	643
	Fbw7	FBW7	-0.408	119		Greatwall	MASTL	-0.098	238
	HRK	HRK	-0.543	17		Mis12	MIS12	-0.560	307
	Omi	HTRA2	-0.257	80		Cap D2	NCAPD2	-0.414	1198
	MULE	HUWE1	-0.278	767		Cap G	NCAPG	-0.383	763
	p38	MAPK14	0.016	550		Cap H	NCAPH	-0.630	632
	JNK1	MAPK8	-0.282	516		Ndc80	NDC80	-0.331	332
	JNK2	MAPK9	-0.143	546		Nde1	NDE1	-0.395	173
	Max	MAX	-0.608	681		Plk1	PLK1	-0.579	1647
	Mcl1	MCL1	-0.312	8220		Securin	PTTG1	-0.153	112
	c-Myc	MYC	-1.085	3168		Sgo1	SGOL1	-0.167	336
Pin1	PIN1	-0.046	245	Ska1	SKA1	-0.331	335		
NOXA	PMAIP1	-1.080	270	Smc1	SMC1A	-0.519	278		
PKA	PRKACA	0.149	794	Smc2	SMC2	-0.477	473		
p53	TP53	-0.379	205	Spindly	SPDL1	-0.303	134		
Tradd	TRADD	0.315	17	SA2	STAG2	-0.194	730		
Usp9X	USP9X	-0.011	934	Megator	TPR	-0.108	435		
XIAP	XIAP	0.128	327	Tpx2	TPX2	-0.460	1236		
MIZ1	ZBTB17	0.223	40	Mps1	TTK	-0.517	338		
				UbcH10	UBE2C	-0.429	3531		
				Wapl	WAPAL	-0.381	779		
				Zw10	ZW10	-0.199	266		

*Values are the mean of 4 biological replicates

A



B



C

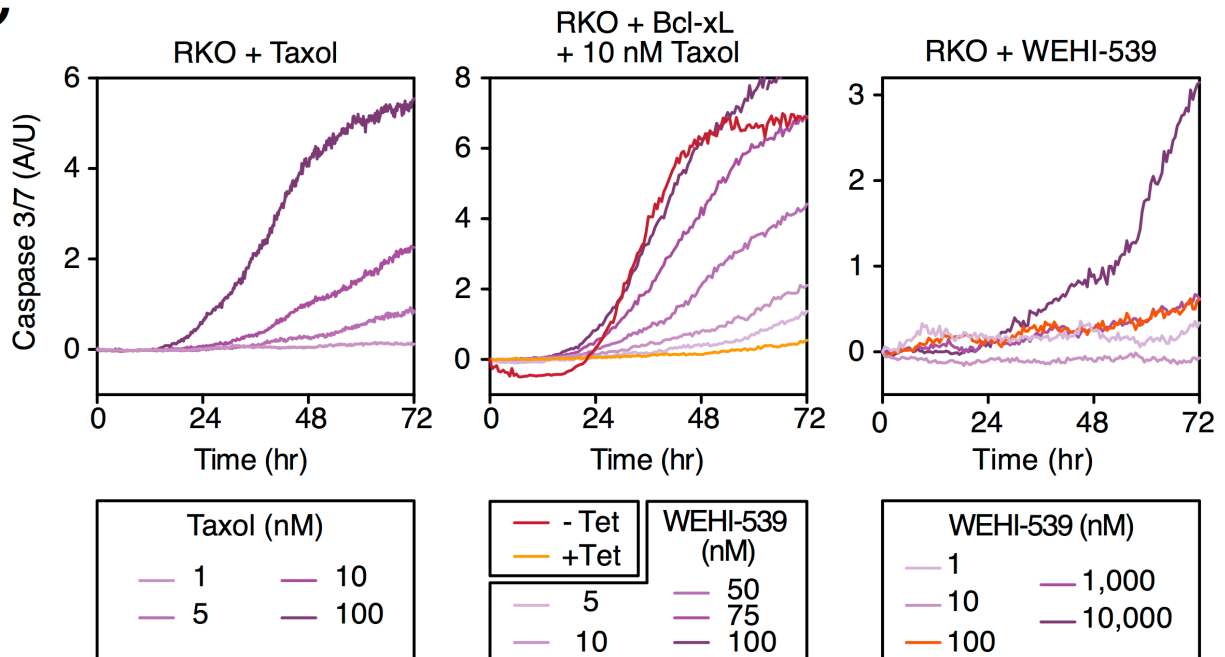


Figure S4, related to Figure 4. Myc promotes post-mitotic death. (A) Immunoblots showing RNAi-mediated inhibition of Myc in the panel of cell lines used in Fig. 4A. Each pair of lanes shows the non-targeting control on the left and the Myc siRNA on the right. (B) Colony formation assay of RKO cells 6 days following exposure to the Mps1 inhibitor AZ3146 for 96 hr. Values represent mean \pm SEM from three independent experiments. (C) Caspase 3/7 assays showing apoptosis induction in RKO cells. Left panel shows a taxol titration. 10 nM was selected for the experiment in Fig. 4D. Middle panel shows that tet-induction of Bcl-xL blocks apoptosis in the presence of 10 nM taxol but that this is reverted by titrating in the Bcl-xL inhibitor WEHI-539. 100 nM was selected for the experiment in Fig. 4D. Right panel shows that in the absence of antimetabolic agents, while 10 μ M WEHI-539 induces apoptosis, 100 nM is relatively benign.

Table S4, related to Figure 4. Effect of c-Myc RNAi in response to 8 antimetabolic agents in 12 cell lines from different tumour types.
 Values represent IncuCyte-based Caspase 3/7 readings (AU) at 96 hrs used to generate Fig. 4A.

Cell Line	Taxol		Nocodazole		Eg5i AZ138		Pik1i BI 2356		Cenp-Ei GSK923295		Aurora Ai MLN8054		Aurora Bi ZM447439		Mps1i AZ3146	
	Ctrl	Myc	Ctrl	Myc	Ctrl	Myc	Ctrl	Myc	Ctrl	Myc	Ctrl	Myc	Ctrl	Myc	Ctrl	Myc
Calu6	510.0	389.5	498.5	338.0	355.5	259.5	479.5	407.0	555.0	350.0	391.5	296.5	464.5	271.5	492.0	177.0
Caov3	501.0	508.5	695.0	429.5	387.0	385.0	525.5	388.0	432.5	458.5	374.0	422.5	342.5	278.5	430.0	492.0
DLD-1	154.0	146.5	129.0	125.5	92.5	56.5	131.5	126.5	142.5	104.0	126.5	176.0	175.0	167.5	228.5	84.5
H1703	307.5	394.0	366.0	403.5	397.5	333.5	255.5	355.5	492.5	539.5	357.5	313.5	355.5	367.0	352.5	275.0
HCT116	367.5	145.5	381.5	127.5	247.5	150.0	289.5	120.0	344.0	119.0	253.0	61.0	175.5	31.0	552.0	223.0
HeLa	149.0	68.5	198.0	142.0	145.0	78.0	128.0	57.5	141.0	76.0	104.0	88.0	110.0	75.5	363.0	157.5
HT29	304.5	156.0	251.0	126.5	187.5	188.0	210.5	113.5	335.5	311.5	212.5	99.0	282.5	76.0	207.0	65.5
MDA	57.0	3.0	32.5	8.0	70.0	8.5	31.5	2.0	37.0	7.0	15.5	-1.0	35.5	1.5	27.5	6.5
PAI	70.0	51.8	37.1	19.6	59.5	30.1	51.8	38.5	70.0	17.5	64.4	23.8	78.4	33.6	61.6	16.8
RKO	452.5	329.5	567.0	205.0	402.0	201.0	272.0	32.0	311.5	272.5	194.5	44.0	143.0	36.0	521.5	45.5
SKOV3	150.5	77.0	65.0	31.0	75.5	57.5	117.5	58.5	83.5	45.0	25.0	12.0	29.0	8.0	37.5	10.5
SW262	20.0	15.5	13.5	9.5	16.0	9.0	20.0	9.0	20.5	10.0	14.0	10.5	13.5	10.5	15.5	10.0

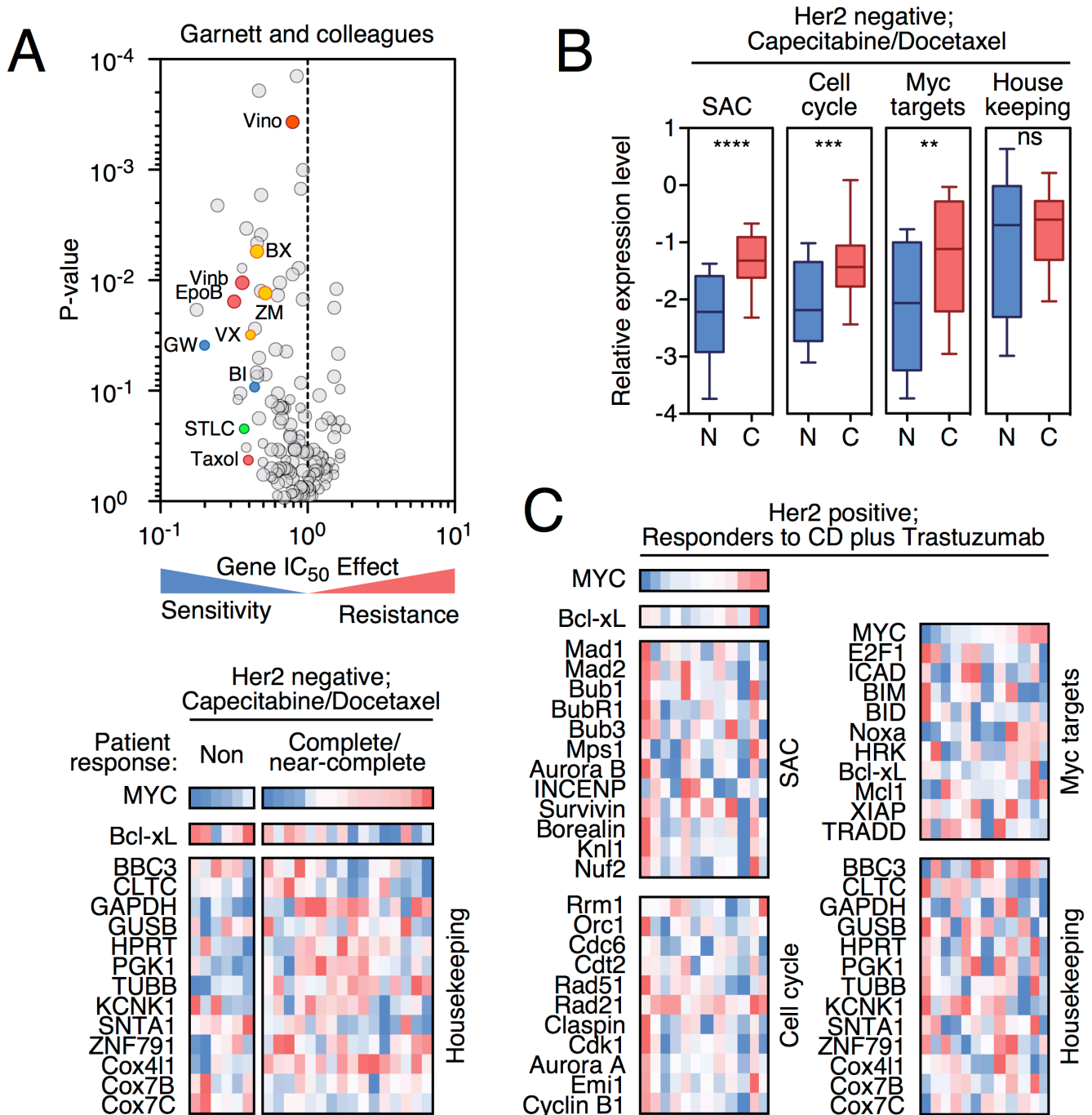


Figure S5, related to Figure 5. Overexpression of Myc sensitizes cancer cells to antimetabolic agents. (A) Volcano plot showing the gene IC_{50} effect and significance (inverted) of *MYC*-drug associations. Each circle represents a single drug effect and the size is proportional to the number of *MYC* overexpressing cell lines screened (range 26-50). Primary data is derived from www.cancerrxgene.org (Garnett et al., 2012; Yang et al., 2013). Taxol, vinorelbine, vinblastine and epothilone B are microtubule inhibitors; BX-795, ZM447439, and VX-680 are Aurora kinase inhibitors; GW843682X and BI-2536 are Plk1 inhibitors; *S*-Trityl-L-cysteine is an Eg5/KSP inhibitor. (B) Box-and-whisker plots (median, interquartile and full range) showing the relative expression levels of SAC, cell cycle and Myc-regulated apoptosis clusters in tumours that either do not respond (N) or show complete/near-complete responses (C) to capecitabine and docetaxel chemotherapy. (C) Heat maps showing gene expression profiles of 12 Her2-positive tumours treated with capecitabine and docetaxel plus Trastuzumab (responders), indicating no obvious correlation with Myc. As in Fig. 5C, each column represents a patient sample and the colour code indicates the relative expression level of the genes indicated, with the sample with the highest value dark red and the lowest value dark blue. Also shown are the housekeeping controls genes to accompany the data in Fig. 5C. Primary data for (B) and (C) are derived from (Glück et al., 2012).

Table S5, related to Figure 5. Gene IC₅₀ effect data for MYC. Used to generate Fig. 5B and S5A.
Source: www.cancerxgene.org. Yang W, et al. Nucleic Acids Research (2013) 41; D955-61.

Drug	Drug Target	Effect	P-value	No. of mutations	Drug	Drug Target	Effect	P-value	No. of mutations
Gemcitabine	DNA replication	0.199	0.020	47	BAY 61-3606	SYK	0.638	0.364	47
GW843682X	PLK1	0.226	0.041	26	Methotrexate	Dihydrofolate reductase (DHFR)	0.642	0.014	50
Thapsigargin	ER Ca ²⁺ ATPase	0.266	0.002	47	Axitinib	PDGFR, KIT, VEGFR	0.642	0.560	50
Epothilone B	Microtubules	0.337	0.016	47	Pazopanib	VEGFR, PDGFRA, PDGFRB, KIT	0.644	0.735	47
CMK	RSK	0.356	0.127	26	OSU-03012	PDK1 (PDKP1)	0.648	0.150	47
Obatoclax	BCL-2, BCL-XL, MCL-1	0.374	0.110	47	Nilotinib	ABL	0.660	0.532	50
Vinblastine	Microtubules	0.387	0.011	50	CEP-701	FLT3, JAK2, NTRK1, RET	0.663	0.206	50
BMS-536924	IGF1R	0.387	0.008	26	AZD7762	CHK1/2	0.664	0.011	50
STLC	KIF11	0.396	0.233	26	AS601245	JNK	0.665	0.381	47
Sumitinib	PDGFRA, PDGFRB, KDR, KIT, FLT3	0.404	0.355	26	OSI-906	IGF1R	0.669	0.143	47
Cisplatin	DNA crosslinker	0.406	0.003	50	PD-0325901	MEK1/2	0.674	0.153	49
Paclitaxel	Microtubules	0.414	0.457	26	AG-014699	PARP1, PARP2	0.687	0.151	49
VX-680	Aurora A/B/C, FLT3, ABL1, JAK2, TOP2	0.437	0.033	26	Docetaxel	Microtubules	0.688	0.186	50
Etoposide	TOP2	0.456	0.029	47	PD-0332991	CDK4/6	0.694	0.995	49
BI-2536	PLK1/2/3	0.464	0.096	26	Bosutinib	SRC, ABL, TEC	0.706	0.538	50
Cytarabine	DNA synthesis	0.467	0.072	50	CCT018159	HSP90	0.710	0.152	49
QS11	ARFGAP	0.468	0.005	47	Elesclomol	HSP70	0.710	0.701	50
BX-795	TBK1, PDK1, IKK, AURKB/C	0.476	0.006	49	GSK-1904529A	IGF1R	0.717	0.047	47
GSK-650394	SGK3	0.480	0.077	47	Pyrimethamine	Dihydrofolate reductase (DHFR)	0.724	0.460	27
GDC-0449	SMO	0.484	0.000	50	Bexarotene	Retinoic acid X family agonist	0.726	0.535	47
GDC0941	PI3K (class 1)	0.485	0.054	49	MK-2206	AKT1/2	0.733	0.555	49
Camptothecin	TOP1	0.493	0.191	50	Parthenolide	NFKB1	0.756	0.127	27
AICAR	AMPK agonist	0.507	0.004	50	SB590885	BRAF	0.759	0.279	49
Vorinostat	HDAC inhibitor Class I, IIa, IIb, IV	0.507	0.013	50	SB 216763	GSK3A/B	0.760	0.213	48
TW 37	BCL-2, BCL-XL	0.510	0.002	49	KU-55933	ATM	0.764	0.583	49
Tipifarnib	Farnesyl-transferase (FNTA)	0.517	0.612	47	JNJ-26854165	MDM2	0.770	0.264	49
BMS-509744	ITK	0.521	0.314	26	GSK269962A	ROCK	0.778	0.920	27
NVP-TAE684	ALK	0.524	0.473	26	AZD6482	PI3Kb	0.783	0.894	47
ZM-447439	AURKB	0.528	0.014	49	CCT007093	PPM1D	0.783	0.474	49
Mitomycin C	DNA crosslinker	0.538	0.076	47	Vinorelbine	Microtubules	0.784	0.000	47
BMS-754807	IGF1R	0.578	0.131	47	LAQ824	HDAC	0.788	0.009	47
AZD6244	MEK1/2	0.579	0.371	49	CI-1040	MEK1/2	0.795	0.683	50
Roscovitine	CDKs	0.583	0.631	27	NU-7441	DNAPK	0.810	0.967	49
ATRA	Retinoic acid receptor agonist	0.583	0.535	50	GW 441756	NTRK1	0.817	0.370	50
JW-7-52-1	MTOR	0.595	0.688	26	AKT inhibitor VIII	AKT1/2	0.820	0.370	47
AZD-2281	PARP1/2	0.619	0.044	50	Lenalidomide	TNF alpha	0.823	0.354	50
MS-275	HDAC	0.628	0.591	27	AUY922	HSP90	0.833	0.000	47
Doxorubicin	DNA intercalating	0.635	0.113	47	IPA-3	PAK	0.838	0.957	47
MG-132	Proteasome	0.637	0.949	27					

ABT-263	BCL2, BCL-XL, BCL-W	0.853	0.303	49
RDEA119	MEK1/2	0.856	0.008	49
RO-3306	CDK1	0.881	0.794	49
VX-702	p38	0.885	0.812	50
Cyclopamine	SMO	0.886	0.269	27
Embelin	XIAP	0.886	0.002	47
A-443654	AKT1/2/3	0.894	0.154	26
JNK-9L	JNK	0.904	0.088	47
Bleomycin	DNA damage	0.905	0.001	47
AZD8055	mTORC1/2	0.909	0.376	49
KIN001-135	IKKE	0.914	0.956	27
PD-173074	FGFR1/3	0.917	0.943	49
PLX4720	BRAF	0.918	0.842	49
EHT 1864	Rac GTPases	0.923	0.574	49
Gefitinib	EGFR	0.924	0.847	50
NVP-BEZ235	PI3K (Class 1) and mTORC1/2	0.926	0.016	49
Nutlin-3a	MDM2	0.950	0.182	49
FH535	unknown	0.971	0.382	47
JNK Inhibitor VIII	JNK	0.975	0.392	49
SL 0101-1	RSK, AURKB, PIM3	0.975	0.814	49
WH-4-023	SRC family, ABL	0.986	0.709	26
Bicalutamide	Androgen receptor (ANDR)	0.990	0.958	47
ABT-888	PARP1/2	0.995	0.837	50
TGX221	PI3K beta	0.999	0.815	27
PF-4708671	p70 S6KA	1.000	0.637	49
Salubrinal	GADD34-PP1C phosphatase	1.030	0.884	27
NSC-87877	SHP1/2 (PTN6/11)	1.050	0.937	47
PF-562271	FAK	1.060	0.368	47
BIRB 0796	p38, JNK2	1.080	0.763	49
Bortezomib	Proteasome	1.090	0.594	27
Bryostatins 1	PRKC	1.090	0.556	47
681640	WEE1, CHK1	1.090	0.472	49

AMG-706	VEGFR, RET, c-KIT, PDGFR	1.110	0.606	49
FTI-277	Farnesyl transferase (FNTA)	1.130	0.566	47
Shikonin	unknown	1.140	0.395	47
CGP-60474	CDK1/2/5/7/9	1.150	0.855	26
Temsirolimus	MTOR	1.170	0.116	50
Lapatinib	EGFR, ERBB2	1.190	0.465	27
CHIR-99021	GSK3B	1.190	0.216	47
BMS-708163	gamma-secretase	1.200	0.432	49
Midostaurin	KIT	1.230	0.545	47
Erlotinib	EGFR	1.240	0.424	23
AZD-0530	SRC, ABL1	1.250	0.764	26
CGP-082996	CDK4	1.260	0.534	26
PAC-1	CASP3 activator	1.260	0.643	47
AZ628	BRAF	1.280	0.610	27
Rapamycin	MTOR	1.300	0.546	26
LFM-A13	BTK	1.310	0.191	47
PF-02341066	MET, ALK	1.360	0.469	26
XMD8-85	ERK5 (MK07)	1.390	0.200	27
17-AAG	HSP90	1.420	0.078	49
A-770041	SRC family	1.430	0.629	26
WZ-184	BMX	1.440	0.542	26
DMOG	Prolyl-4-Hydroxylase	1.440	0.018	47
AP-24534	ABL	1.440	0.283	47
AZD6482	PI3Kb (P3C2B)	1.470	0.012	47
Imatinib	ABL, KIT, PDGFR	1.490	0.240	26
BIBW2992	EGFR, ERBB2	1.510	0.048	50
Z-LLNle-CHO	g-secretase	1.560	0.103	26
PHA-665752	MET	1.570	0.196	26
GNF-2	BCR-ABL	1.580	0.405	26
Dasatinib	ABL, SRC, KIT, PDGFR	1.580	0.440	26
Sorafenib	PDGFRA, PDGFRB, KDR, KIT, FLT3	1.690	0.234	27

Notes: The volcano plot (Fig. S5A) visualises the correlation of drug sensitivity data with genetic events calculated using a multivariate ANOVA. Gene specific volcano plots represent the effect of a mutated gene (e.g. BRAF) on the responses to all drugs analysed. The volcano plot presents three pieces of data:

- x-axis: The magnitude of the effect that genetic events have on cell lines IC₅₀ values in response to a drug. IC₅₀ values were correlated with the status of commonly altered cancer genes using a two way multivariate ANOVA, with mutation status and tissue type as factors. The effect size is proportional to the difference in mean IC₅₀ between wild-type and mutant cell lines. Numbers less than 1 indicate drug sensitivity, numbers greater than 1 indicate drug resistance.
- y-axis: The p-value from the MANOVA of a drug-gene interaction on an inverted log10 scale.
- Size of each circle: The number of genetic events contributing to the analysis for a given gene or drug.

(See www.cancerrxgene.org for more details.)

Table S6, related to Figure 5. Gene expression profiles and patient responses to Capecitabine/Docetaxel chemotherapy. Used to generate Fig. 5C and S5C.
Source: www.oncomine.org. Glück et al (2012) Breast Cancer Res Treat. 132(3):781-91.

Sample Number	35	34	37	33	32	36	124	113	117	125	123	114	110	119	118	122	112	111	116	115	121	120
Response	N	N	N	N	N	N	CR	NC	CR	CR	CR	NC	NC	CR	CR	CR	NC	NC	CR	NC	CR	CR
Aurora A	-2.66	-1.56	-2.51	-2.76	-3.17	-3.25	-3.06	-2.12	-3.62	-0.45	-1.72	-2.34	-1.78	-1.86	-1.57	-1.37	-1.32	-0.79	-1.68	-2.82	-1.23	-0.40
Aurora B	-2.31	-1.71	-1.94	-2.00	-2.12	-1.56	-2.01	-1.64	-2.07	-1.90	-1.69	-2.07	-1.74	-1.66	-1.18	-0.85	-0.62	-0.95	-2.03	-2.46	-0.78	-0.64
BBC3	0.09	-0.06	0.34	0.13	0.18	-0.23	0.26	0.06	-0.03	0.45	0.03	0.10	-0.26	-0.04	-0.39	-0.31	0.04	0.00	0.15	-0.18	-0.16	-0.41
Bel-xL	0.18	0.10	-0.62	-0.24	-0.14	0.25	-0.05	-0.35	0.04	-0.09	-0.37	-0.15	-0.49	-0.14	-0.69	-0.33	-0.46	-0.74	-0.71	0.05	-0.63	-0.39
Bid	-0.43	0.43	-0.91	-0.51	-0.92	-1.19	0.13	-0.01	-1.49	-0.54	0.22	-0.27	0.27	0.88	0.74	0.92	0.53	-0.10	-0.04	-0.49	0.18	0.34
Bim	-0.45	-0.43	-0.39	-0.84	-0.94	-0.80	-0.90	-0.63	-0.67	-0.66	-0.17	-0.42	-0.29	-0.03	-0.53	-0.14	-0.66	0.62	-0.85	-0.73	-0.14	0.50
Borealin	-2.63	-1.38	-2.31	-2.11	-2.69	-3.19	-2.54	-1.09	-3.30	-0.76	-0.49	-1.99	-1.92	-1.55	-0.47	-1.33	-1.13	-1.25	-1.38	-2.44	-0.41	0.32
Bub1	-3.37	-1.81	-3.76	-3.17	-3.70	-4.66	-3.69	-2.27	-5.04	3.03	-1.91	-2.48	-1.45	-1.84	-1.18	-1.39	-2.08	-1.23	-2.33	-3.86	-1.99	-0.85
Bub3	-2.09	-1.52	-0.90	-0.62	-1.42	-2.17	-1.22	-1.23	-1.11	-0.27	0.04	-0.84	-1.38	-0.75	-0.91	-0.73	-1.33	1.03	-1.03	-1.46	0.39	-0.48
BubR1	-1.64	-1.07	-3.36	-1.78	-2.39	-2.07	-2.26	-2.15	-1.97	-2.30	-1.93	-1.47	-1.07	-1.85	-1.44	-1.33	-1.40	-1.93	-1.72	-2.11	-0.93	-0.37
Cdc6	-2.57	-2.71	-3.03	-2.98	-2.87	-3.77	-3.68	-2.76	-3.75	0.29	-1.52	-2.85	-1.39	-1.55	-1.86	-2.18	-1.68	-1.82	-2.76	-3.65	-2.24	-1.36
CDK1	-3.30	-2.18	-2.64	-2.54	-3.81	-4.14	-2.66	-1.99	-4.35	-1.46	-1.75	-1.69	-1.64	-0.78	-0.50	-0.14	-1.24	-0.67	-1.11	-3.10	-0.81	-1.00
Cdt2	-1.50	0.63	-1.32	-2.01	-2.61	-3.22	-2.51	-1.81	-3.41	-1.39	-0.83	-1.99	-2.05	-1.17	-0.99	0.04	-0.88	0.07	-0.96	-2.06	-2.17	-0.69
Claspin	-0.93	-0.42	-1.20	-0.90	-1.36	-1.28	-1.23	-1.02	-2.10	-0.21	-0.89	-0.84	-0.60	0.09	-1.05	-0.67	-1.49	0.16	-1.20	-1.48	-0.02	-0.10
CLTC	-0.51	-0.23	-0.34	-0.57	-0.33	-0.82	0.00	0.50	2.79	-0.07	-0.33	-0.61	-0.26	-0.67	-0.85	-0.70	-0.35	1.49	-0.68	-0.77	-0.60	-0.91
Cox4I1	-1.68	-2.14	-0.47	-0.79	-1.00	-0.92	-0.12	-0.45	-0.48	-0.12	-0.58	-0.22	-0.99	-0.03	-0.38	0.24	0.27	-0.04	-0.33	-0.85	0.09	-0.54
Cox7B	0.35	2.24	-0.54	-0.15	-0.86	0.55	-0.18	-0.73	-0.70	0.79	0.12	-0.50	-0.01	0.75	-0.03	0.35	-1.69	0.37	-0.08	0.06	0.36	-0.06
Cox7C	1.30	2.10	-0.07	0.08	-0.16	0.99	-0.26	-0.68	0.03	0.04	-0.34	-0.19	-0.91	-0.58	-0.53	-0.06	-0.88	0.24	-0.40	0.36	-0.24	-0.43
E2F1	-1.46	-0.75	-1.92	-2.06	-2.63	-2.43	-1.84	-0.97	-2.53	-1.08	0.18	-1.44	-0.95	0.11	-0.14	-0.25	-1.29	-0.52	-0.20	-1.58	-1.18	-0.03
Emil	-2.42	-2.19	-2.48	-1.58	-2.05	-3.31	-2.21	-1.99	-2.99	-1.69	-0.73	-1.28	-0.72	-1.29	-1.36	-1.12	-1.64	-1.51	-1.58	-2.62	-0.41	0.13
GAPDH	-1.94	-2.58	-1.69	-1.94	-2.39	-2.58	-1.87	-1.88	-2.41	-0.78	-0.49	-0.50	-1.20	-0.97	-0.68	-0.90	-1.50	-2.07	-1.30	-2.45	-0.56	-0.95
GUSB	0.35	-0.58	-0.14	0.54	0.17	0.33	0.73	-0.17	0.07	-0.03	0.19	0.35	-0.08	-0.22	0.52	0.16	0.02	0.17	0.11	0.81	-0.17	-0.33
HPRT	-1.42	0.33	-1.26	-1.58	-1.65	-2.85	-1.20	-1.89	-1.86	-0.24	-0.10	-0.66	-0.99	0.79	-0.54	-0.11	-0.60	-0.27	-0.64	-1.78	-1.06	-0.55
HRK	-0.34	-0.34	0.01	-0.67	-0.42	-0.74	0.20	-0.03	-0.84	0.23	1.74	0.78	0.53	0.32	-0.41	-0.04	-0.21	-0.26	-0.46	-0.14	0.93	0.46
ICAD	-1.10	-1.17	-0.97	-0.57	-0.91	-1.46	-0.80	-0.71	-1.59	-1.19	-0.49	-0.70	-1.17	-0.11	-0.04	0.14	-0.26	-0.92	-0.24	-0.95	-0.06	0.54
INCENP	-1.27	0.26	-2.58	-1.39	-1.87	-2.03	-1.55	-0.08	-2.86	-1.25	0.38	-0.94	-1.08	-1.16	-0.58	0.78	0.60	-0.69	0.00	-1.19	-0.33	-0.75
KCNK1	3.02	0.24	2.71	-1.12	-0.64	-0.75	0.34	1.37	-2.02	1.09	2.41	1.44	1.21	1.46	1.26	1.91	-0.70	-2.22	-0.23	0.36	0.91	-1.94
KnI1	-2.21	-0.82	-2.01	-1.96	-1.98	-2.57	-2.61	-1.76	-2.96	-1.65	-1.33	-1.71	-1.43	-1.37	-1.84	-0.63	-1.22	-0.73	-1.32	-2.40	-1.02	-0.97
Mad1	-1.79	-1.62	-1.13	-0.87	-1.19	-1.63	-0.87	-0.87	-1.03	-0.47	-0.87	-0.85	-1.30	-0.49	-1.04	-0.89	-0.13	0.39	-1.14	-1.58	-1.12	-0.86
Mad2	-5.03	-3.59	-2.95	-2.26	-3.09	-5.54	-2.94	-2.69	-4.16	-1.54	-1.55	-1.62	-1.82	-1.37	-1.25	-1.11	-0.68	-0.75	-0.94	-3.89	-0.79	-0.72
McI1	-0.66	-1.25	0.02	0.15	-0.29	-0.48	0.10	1.09	-0.69	0.34	0.95	0.00	1.23	0.56	0.81	0.03	0.63	0.39	0.66	-0.16	0.41	1.34
Mps1	-2.54	-1.86	-3.28	-2.11	-2.79	-3.60	-3.22	-2.21	-3.74	-1.48	-0.57	-1.59	-0.90	-1.20	-0.28	-0.27	-0.15	-0.15	-1.14	-3.36	-1.12	0.35
MYC	-3.20	-3.11	-2.91	-2.78	-2.55	-2.17	-3.18	-3.07	-2.96	-2.84	-2.24	-1.91	-1.91	-1.67	-1.20	-1.05	-1.02	-0.88	-0.77	-0.51	0.38	1.37
Noxa	-1.98	-2.25	-2.68	-2.01	-0.28	-3.69	-1.47	-3.40	-4.13	-1.71	-0.66	-2.26	-1.74	-3.29	-1.67	-4.12	-1.52	-1.18	-2.31	-2.55	-2.25	-0.38
Nuf2	-3.17	-1.50	-2.44	-2.73	-3.27	-3.97	-2.60	-1.31	-3.50	-2.76	-0.72	-1.43	-0.67	-1.36	-0.16	-0.63	-0.41	-0.49	-0.66	-2.71	-0.45	1.24
Orc1	-1.80	-2.44	-2.39	-2.15	-2.18	-1.35	-1.96	-2.44	-2.71	-1.97	-0.57	-2.15	-1.46	-1.32	-1.93	-2.02	-0.90	-2.49	-2.78	-1.99	-1.02	-1.27
PGK1	-1.34	-1.87	-2.22	-2.04	-2.44	-2.24	-1.57	-1.90	-2.56	-1.09	-1.00	-0.19	-1.15	-1.06	-1.11	-0.65	-1.58	-1.69	-1.78	-2.10	-1.39	-1.96

Sample Number	35	34	37	33	32	36
Response ¹	N	N	N	N	N	N
Rad21	-1.71	-1.38	-0.77	-0.58	-0.26	-1.66
Rad51	-2.31	-0.92	-2.56	-2.00	-2.89	-3.25
Rrm1	-2.18	-1.52	-0.97	-0.61	-1.38	-1.98
SNTA1	-0.14	-0.04	0.05	-0.14	-0.01	0.61
Survivin	-3.17	-1.57	-3.14	-1.96	-3.47	-4.38
TRADD	-2.44	-2.37	-0.77	-0.90	-0.90	-2.29
TUBB	-2.50	-2.45	-1.53	-1.35	-1.39	-2.07
XIAP	0.60	-0.45	1.89	-0.75	0.23	0.27
ZNF791	-0.93	-1.06	0.00	0.05	0.35	-0.55

	124	113	117	125	123	114	110	119	118	122	112	111	116	115	121	120
	CR	NC	CR	CR	CR	NC	NC	CR	CR	CR	NC	NC	CR	NC	CR	CR
	0.16	0.05	1.35	-1.09	0.25	-0.16	-0.97	-0.03	-0.11	-0.20	0.52	0.37	0.80	-0.43	0.46	0.47
	-2.32	-1.81	-3.47	-1.53	-0.78	-2.36	-0.66	-1.16	-0.99	-0.49	-0.32	-0.52	-1.42	-2.61	-1.86	-0.46
	-1.82	-1.23	-1.83	-1.29	-1.07	-1.76	-0.62	-1.82	-0.56	-0.77	-0.47	-0.77	-1.74	-1.19	-0.84	-0.52
	-0.20	-0.25	0.00	0.13	-0.46	0.04	-0.09	-0.55	-0.50	-0.34	-0.45	-0.81	-0.60	0.47	-0.61	-0.73
	-3.12	-1.11	-3.49	-1.33	-1.37	-0.85	-1.78	-1.45	-0.97	-1.35	0.92	0.51	-2.18	-2.58	1.20	-0.94
	-0.25	0.00	-0.89	-0.38	-0.04	-0.62	-0.47	-0.17	-0.47	-0.55	1.11	-0.65	-0.52	-1.55	-0.47	-0.15
	-1.18	-0.41	-1.77	-1.09	-1.30	-1.35	-0.77	-1.07	-0.44	-0.68	-0.73	-1.73	-0.63	-1.72	0.00	-0.47
	0.02	-0.33	0.33	1.26	0.72	0.91	0.48	1.34	0.00	0.35	-1.28	0.93	0.86	-0.32	0.33	0.11
	-0.27	0.60	0.65	-0.05	-0.16	-0.63	0.15	0.35	-0.21	-0.30	-0.07	-0.96	0.07	-0.01	0.38	0.48

Values represent Log2 median-centered ratio.

¹ Patient treatment response: N, no response; NC, near complete response; CR, complete response.

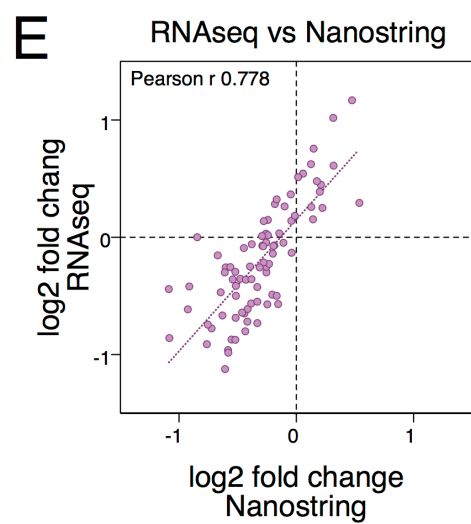
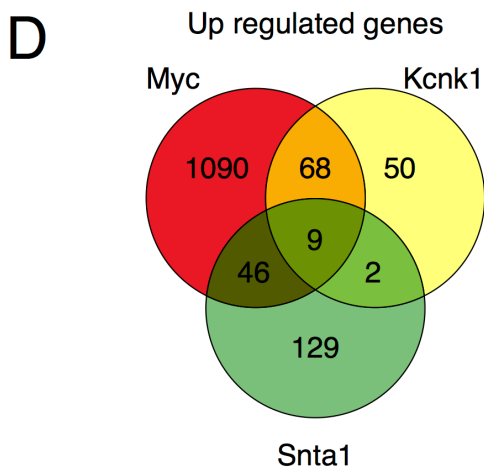
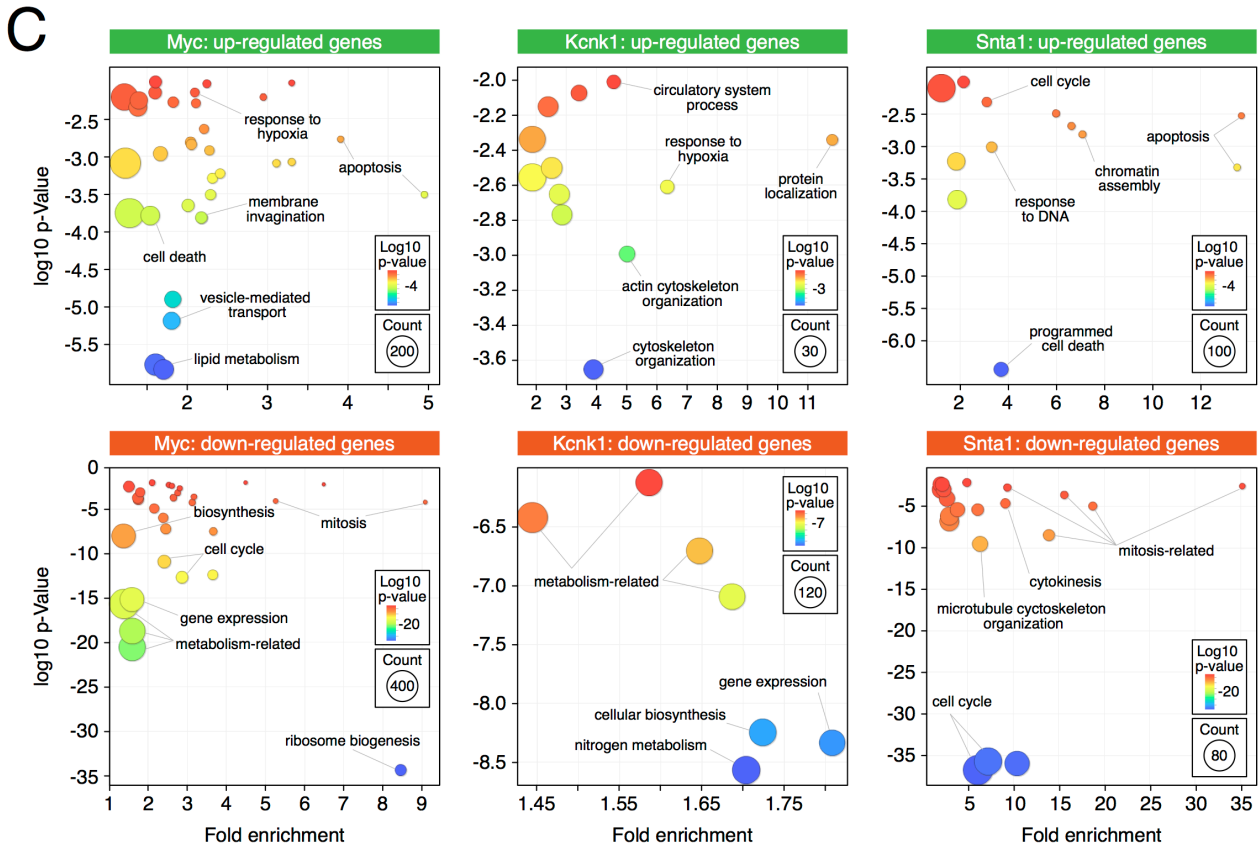
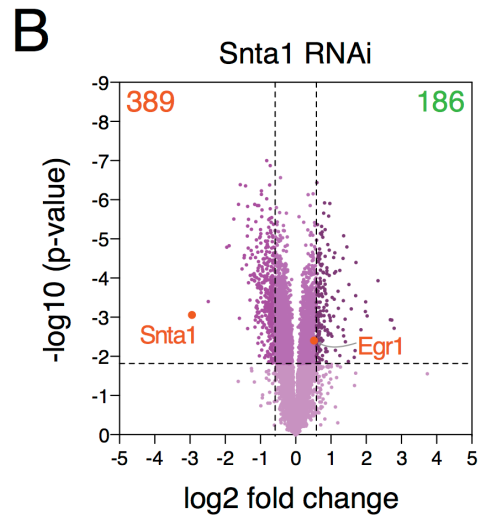
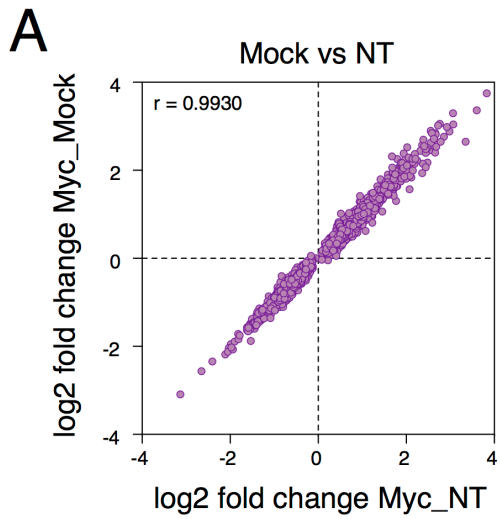
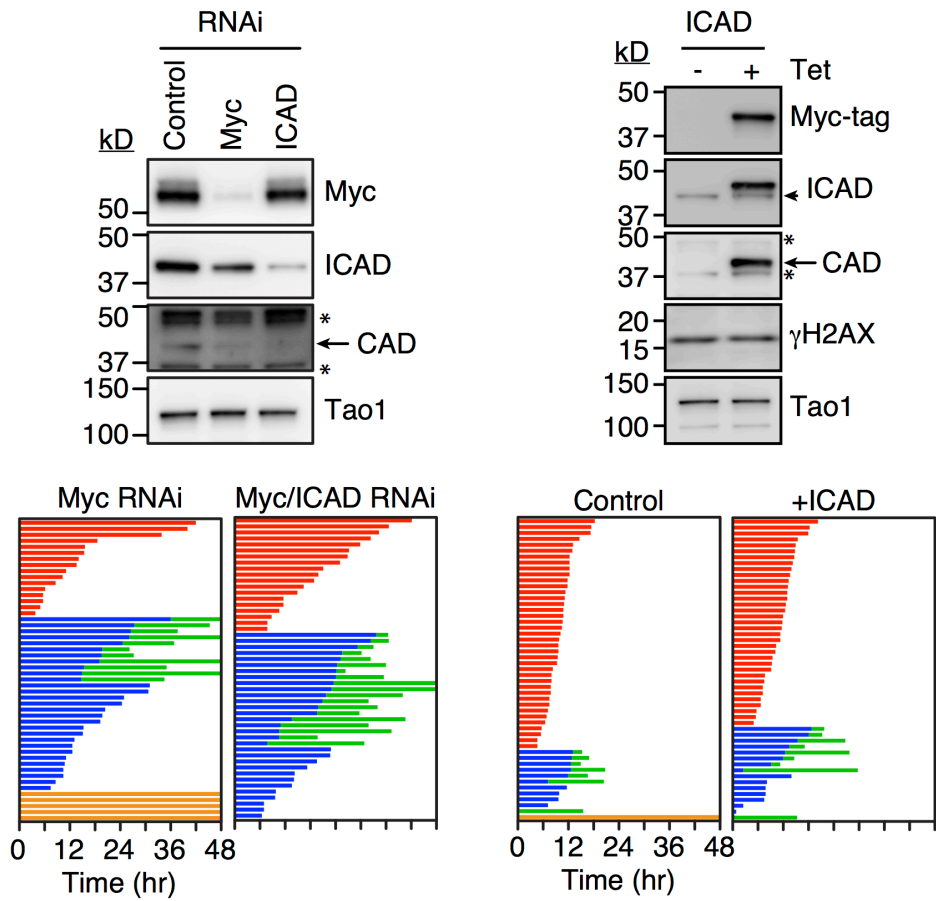


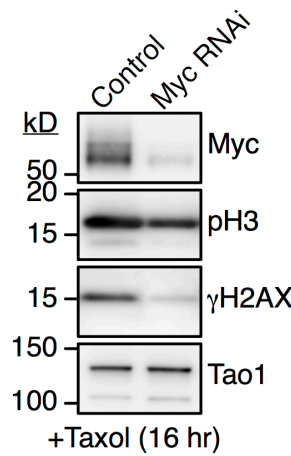
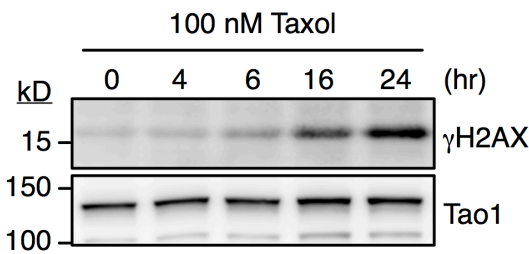
Figure S6, related to Figure 7. Global gene expression profiling. (A) Gene expression fold changes following Myc RNAi, normalized to either mock transfected (y -axis) or cells transfected with a non-targeting control siRNA (x -axis). Each value is the average derived from five biological replicates for mock and four each for the non-targeting control and Myc siRNA. Because of the excellent correlation, all subsequent analysis was performed with values normalized to the non-targeting control siRNA. (B) Volcano plot showing the gene expression changes induced by transfection of *SNTA1* siRNA #4. (C) Gene ontology analysis of the up and downregulated genes following transfection of siRNAs targeting Myc, Kcnk1 and Snta1. Gene Ontology analysis was performed with DAVID Bioinformatics Resources 6.7 (Huang da et al., 2009) then visualized with Revigo (Supek et al., 2011). The Snta1 siRNA deregulated 575 genes, with *SNTA1* itself the most repressed gene. Cell cycle and mitosis-related gene ontology terms feature heavily, consistent with this siRNA accelerating mitotic exit. Interestingly, FoxM1, which drives G2/M gene expression was reduced 1.75-fold (not shown), indicating that this siRNA may disrupt mitotic controls by deregulating FoxM1 (Laoukili et al., 2005). (D) Venn diagram showing the number of common upregulated genes. (E) Fold changes for the genes analyzed in Fig. 3A showing good correlation between the Nanostring and RNAseq-based measurements.

Table S7, related to Figure 7. RNA-Seq-derived gene expression analysis. Used to generate Fig. 7A and S6B. (Provided as an Excel file).

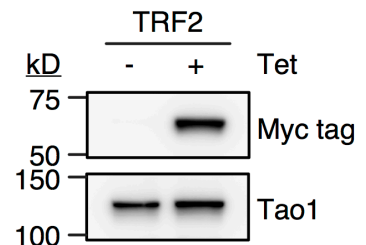
A



B



D



C

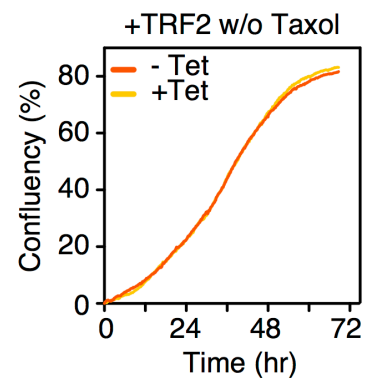
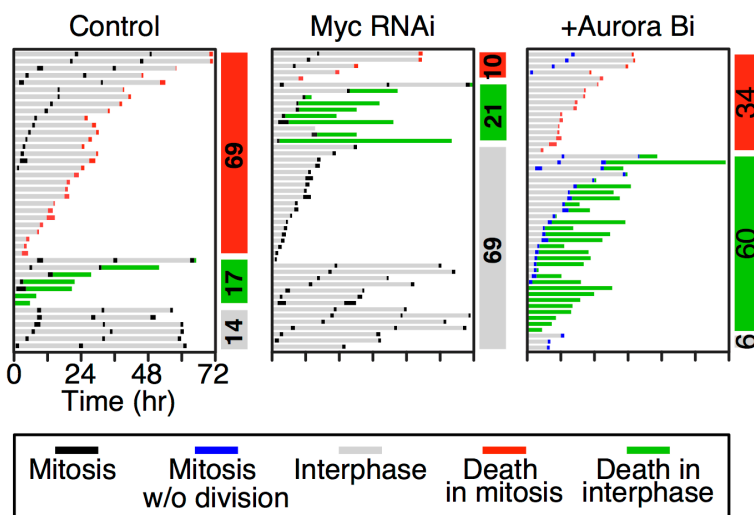


Figure S7, related to Figure 8. Inhibition of ICAD/CAD and telomere deprotection enhances slippage. (A) Characterisation of ICAD RNAi and overexpression. Immunoblots show that inhibition of either Myc or ICAD reduces CAD levels. Fate profiles show that RNAi-mediated inhibition of ICAD in Myc RNAi cells does not further suppress DiM. Tet-induced overexpression of ICAD elevates levels of CAD but this has no obvious effect on DNA damage or DiM. Asterisks mark non-specific bands. (B) Immunoblot shows that taxol exposure induces γ H2AX, indicating DNA damage, and that this is suppressed by Myc RNAi. (C) Fate profiles of RKO cells in the absence of taxol following RNAi-mediated co-repression of Bcl-xL and Mcl1. In contrast to fate profiles of taxol-treated cells, here, zero hr represents when imaging started as opposed to when the cell first entered mitosis. 69% of Bcl-xL/Mcl1-deficient cells undergo DiM, indicating that in the absence of pro-survival function, mitosis is a significant stress, inducing apoptosis without the addition of taxol. Co-repression of Myc reduces DiM in Bcl-xL/Mcl1-deficient cells to 10%, consistent with Myc counterbalancing pro-survival function. Exposing Bcl-xL/Mcl1-deficient cells to 2 μ M ZM447439, a selective Aurora B inhibitor (Ditchfield et al., 2003), also reduces DiM in the absence taxol, to 34%. Note that Aurora B promotes telomere deprotection upon mitotic entry, activating a DNA damage signal (Hayashi et al., 2012). (D) Characterisation of a tet-inducible RKO cell line overexpressing the shelterin component TRF2, tagged with an N-terminal Myc epitope. Immunoblot shows induction of TRF2 with 1 μ g/ml tetracycline and growth curves shows that, in the absence of taxol, this does not inhibit proliferation.

Supplemental Experimental Procedures

Cell lines

Colon carcinoma lines (RKO, DLD-1, HCT116, HT29), lung carcinoma lines (Calu6 and H1703) breast (MDA-MB-231) and ovarian cancer lines (SKOV3, PA1, SW626, Caov3) were obtained from the American Type Culture Collection. HeLa cells were as described (Taylor and McKeon, 1997), HCT116 p53^{-/-} were provided by Bert Vogelstein (Bunz et al., 1998). Cells were cultured in DMEM plus 10% fetal calf serum (LifeTechnologies), 2 mM glutamine, 100 U/ml penicillin, and 100 U/ml streptomycin (Lonza). For PA1, SW626 and SKOV3, DMEM was replaced by Minimum Essential Media, Leibovitz's L-15 (Sigma-Aldrich) and McCoy's (modified) 5A medium (Life Technologies) respectively. All lines were grown at 37°C in a humidified 5% CO₂ incubator. For the tertiary screen, we use an RKO line expressing a GFP-tagged histone H2B (Gascoigne and Taylor, 2008) so that mitotic index could be approximated by measuring the granularity of the chromatin.

siRNA sequences

The sequences of siRNAs used in this study are listed below. All siRNAs were from Dharmacon unless stated otherwise.

Target	siRNA sequence	Notes
Bcl-2	GGGAGAACAGGGUACGAUA GAAGUACAUCUUAUAAG GGAGGAUUGUGCCUUCUU UCGCCGAGAUGUCCAGCCA	
Bcl-xL	GGACAGCAUAUCAGAGCUU GAAAUGACCAGACACUGAC CCUACAAGCUUCCAGAA UUAGUGAUGUGGAAGAGAA	
Bid	GGGAUGGACUGAACGGACA CUAGAGACAUGGAGAAGGA GCACCUACGUGAGGAGCUU GUAACUAACUGCAUACACU	
Bim	UGACCGAGAAGGUAGACAA CAACCACUAUCUCAGUGCA	Life Technologies
BubR1	AACGGGCAUUUGAAUAUGAAA	Positive control siRNA in library screen. (Ditchfield et al., 2003)
Egr1	GAUGAACGCAAGAGGCAUA CGACAGCAGUCCCAUUUAC GGACAUGACAGCAACCUUU GACCUGAAGGCCCUCAAUA	
Myc	#4 CGAUGUUGUUUCUGUGGAA #5 AACGUUAGCUUCACCAACA #6 GGAACUAUGACCUCGACUA #8 CUACCAGGCUGCGCGCAA	These four siRNAs were pooled for routine use while #4 was used in isolation for the RNAi-rescue experiment (Fig. S2B).
G1	siGLO RISC-free siRNA (D-001600-01-05)	Additional negative control siRNA (Fig. S2A).
GAPDH (GA)	UGGUUUACAUGUCCAAUA	Negative control siRNA in library screen.
Hrk	GGGAAGCCCUUUGGAAAUC GAUCGUAGAAACACAGAAU UCAAGGCGCUAGGCGACGA AGGCGGAACUUGUAGGAAC	
ICAD	GGCGAGAUCGGACUCUAA GACAUUCUGGCCAUUGAUA ACGCAGAGCUUGCAUUCUC GAAAGAAGAUCUGUCCAGC	

KCNK1	#6	CGGUGGAGCUGCCCUAUGA	Active siRNA (Fig. S1)
Mcl1		CGAAGGAAGUAUCGAAUUU GAUUAUCUCUCGGUACCUU GAAGGUGGCAUCAGGAAUG GGUUUGGCAUAUCUAAUAA UGGUUUACAUGUCGACUAA	
Non-targeting (NT)		UGGUUUACAUGUUGUGUGA UGGUUUACAUGUUUUCUGA UGGUUUACAUGUUUCCUA	Routine negative control siRNA pool.
Noxa		AAACUGAACUCCGGCAGA GAACCUGACUGCAUAAAA AAUCUGAUAUCCAAACUCU GCAAGAACGCUCAACCGAG	
Scramble (SC)		AAAACCAUCAUACCAGAGACA	Additional negative control siRNA (Fig. S2A).
SNTA1	#4	CAGAUUGGCUGGCUAACUG	Active siRNA (Fig. S1D)
Tao1 (T1)		GUAUAUGGUCCUUUCUAA	Additional negative control siRNA (Fig. S2A). (Westhorpe et al., 2010)
XIAP		GUAGAUAGAUGGCAAUAUG GAACUGGGCAGGUUGUAGA GAAAGAGAUUAGUACUGAA GGACUCUACUACACAGGUA	
ZNF791	#1	GGGAAGACCCGAAUGUUGA	Active siRNA (Fig. S1D)

cDNAs

Open reading frames were generated either by using SuperScript One-Step RT-PCR with mRNA prepared from HeLa or RKO cells, or PCR amplified using Pfu Turbo with a plasmid as the template, then cloned into a pcDNA5/FRT/TO-based vector modified to include an N-terminal Myc or GFP epitope tag (Girdler et al., 2006). Myc and Omomyc were engineered with a C-terminal GFP tag, XIAP, Bcl-xL, ICAD and TRF2 were tagged with a Myc epitope at the N-terminus, and Bim was untagged. All ORFs were verified by sequencing.

Name	Accession	PCR primers (5' - 3')	Source
Bcl-xL	NM_138578.1	TCTCAGAGCAACCGGGAGCTG TCATTTCCGACTGAAGAGTGAG	RT-PCR
Bim	NM_138621.4	ATGGCAAAGCAACCTTCTG TCAATGCATTCTCCACACC	Thermo Scientific Clone ID 5213713
Myc	NM_002467.4	ATGCCCTCAACGTTAGCTTC CGCACAAGAGTTCCGTAG	RT-PCR
ICAD	NM_004401.2	GAGGTGACCGGGACGCCGGG CTATGTGGGATCCTGTCTGGC	RT-PCR
TRF2	NM_005652	GCGGGAGGAGGCCGGGAGTAGC TCAGTTCATGCCAAGTC	Addgene 16066 (Karlseder et al., 2002)
XIAP	NM_001167.3	ACTTTTAAACAGTTTTGAAGG TTAAGACATAAAAATTTTTGCTTG	RT-PCR
Omomyc		ATGGAGGAGAATGTCAAG CGCACAAGAGTTCCGTAG GTTGCGGAAACAAAACGAACAGTTGA TCAACTGTTTCGTTTTGTTCCGCAAC CAAGCAGAGACGAAAAGCTCATTCTGA -AATCGACTTGTTG CAACAAGTCGATTTTCAGAAATGAGCTTTT- GCGTCTC	(Soucek et al., 1998)

Antibodies

Primary antibodies for immunoblotting are listed below.

Antigen	Antibody name	Source/ Citation
Bcl-xL	Rabbit anti-Bcl-xL	Cell Signaling Technology
Bcl2	Mouse anti-Bcl2	BD Biosciences
Bid	Rabbit anti-Bid (Human specific)	Cell Signaling
Bim	Rabbit anti-Bim	BD Biosciences
Bub3	Sheep anti-Bub3	Holland and Taylor, unpublished
BubR1	Sheep anti-BubR1 (SBR1.1)	(Taylor et al., 2001)
Caspase 3	Mouse anti-caspase 3	Cell Signaling
Egr1	Rabbit anti-Egr1 (588)	Santa Cruz
γ H2AX	Rabbit anti- γ H2Ax	Novus Biologicals
pH3-Ser10	Rabbit anti-Histone H3 pSerine10	Millipore
Myc	Rabbit anti-c-Myc (Y69)	AbCam
CAD	Rabbit anti-DFFB	Sigma
HRP anti-sheep/ mouse/ rabbit	Conjugated secondaries	Invitrogen
ICAD	Rabbit anti-ICAD	AbCam
Mcl1	Rabbit anti-Mcl1 (S-19)	Santa Cruz Biotechnology
Myc epitope tag	4A6	Millipore
Noxa	Mouse anti-Noxa (114C307)	Merck Millipore
Tao1	Sheep anti-Tao1	(Westhorpe et al., 2010)
XIAP	Rabbit anti-XIAP	Cell Signaling Technology

Small molecule inhibitors

Small molecule inhibitors were dissolved in DMSO and stored at -20°C, except tetracycline which was dissolved in water.

Name	1° Target	Concentration	Source/ Citation
AZ138	Eg5/KSP	1 μ M	AstraZeneca (Gascoigne and Taylor, 2008)
AZ3146	Mps1	2 μ M	AstraZeneca (Hewitt et al., 2010)
BI2536	Plk1	100 nM	Boehringer Ingelheim (Steehmaier et al., 2007)
GSK923295	Cenp-E	100 nM	(Wood et al., 2010), (Bennett et al., in preparation)
JQ1	Brd4	0.5 μ M	Stefan Knapp (Filippakopoulos et al., 2010)
MLN8054	Aurora A	1 μ M	Millennium Pharmaceuticals (Manfredi et al., 2007)
Nocodazole	Microtubules	30 ng/ml	Sigma
Taxol	Microtubules	100 nM	Sigma
Tetracycline	Tet repressor	See legends	Sigma
WEHI-539	Bcl-xL	100 nM	Apexbio (Lessene et al., 2013)
ZM447439	Aurora B	2 μ M	Tocris (Ditchfield et al., 2003)

Supplemental References

- Bunz, F., Dutriaux, A., Lengauer, C., Waldman, T., Zhou, S., Brown, J. P., Sedivy, J. M., Kinzler, K. W., and Vogelstein, B. (1998). Requirement for p53 and p21 to sustain G2 arrest after DNA damage. *Science* *282*, 1497-1501.
- Chung, N., Zhang, X. D., Kreamer, A., Locco, L., Kuan, P. F., Bartz, S., Linsley, P. S., Ferrer, M., and Strulovici, B. (2008). Median absolute deviation to improve hit selection for genome-scale RNAi screens. *J Biomol Screen* *13*, 149-158.
- Ditchfield, C., Johnson, V., Tighe, A., Ellston, R., Haworth, C., Johnson, T., Mortlock, A., Keen, N., and Taylor, S. S. (2003). Aurora B couples chromosome alignment with anaphase by targeting BubR1, Mad2, and Cenp-E to kinetochores. *J Cell Biol* *161*, 267-280.
- Girdler, F., Gascoigne, K. E., Eyers, P. A., Hartmuth, S., Crafter, C., Foote, K. M., Keen, N. J., and Taylor, S. S. (2006). Validating Aurora B as an anti-cancer drug target. *J Cell Sci* *119*, 3664-3675.
- Hewitt, L., Tighe, A., Santaguida, S., White, A. M., Jones, C. D., Musacchio, A., Green, S., and Taylor, S. S. (2010). Sustained Mps1 activity is required in mitosis to recruit O-Mad2 to the Mad1-C-Mad2 core complex. *J Cell Biol* *190*, 25-34.
- Huang da, W., Sherman, B. T., and Lempicki, R. A. (2009). Systematic and integrative analysis of large gene lists using DAVID bioinformatics resources. *Nat Protoc* *4*, 44-57.
- Karlseder, J., Smogorzewska, A., and de Lange, T. (2002). Senescence induced by altered telomere state, not telomere loss. *Science* *295*, 2446-2449.
- Laoukili, J., Kooistra, M. R., Bras, A., Kauw, J., Kerkhoven, R. M., Morrison, A., Clevers, H., and Medema, R. H. (2005). FoxM1 is required for execution of the mitotic programme and chromosome stability. *Nat Cell Biol* *7*, 126-136.
- Manfredi, M. G., Ecsedy, J. A., Meetze, K. A., Balani, S. K., Burenkova, O., Chen, W., Galvin, K. M., Hoar, K. M., Huck, J. J., LeRoy, P. J., *et al.* (2007). Antitumor activity of MLN8054, an orally active small-molecule inhibitor of Aurora A kinase. *Proc Natl Acad Sci U S A* *104*, 4106-4111.
- Soucek, L., Helmer-Citterich, M., Sacco, A., Jucker, R., Cesareni, G., and Nasi, S. (1998). Design and properties of a Myc derivative that efficiently homodimerizes. *Oncogene* *17*, 2463-2472.
- Steegmaier, M., Hoffmann, M., Baum, A., Lenart, P., Petronczki, M., Krssak, M., Gurtler, U., Garin-Chesa, P., Lieb, S., Quant, J., *et al.* (2007). BI 2536, a potent and selective inhibitor of polo-like kinase 1, inhibits tumor growth in vivo. *Curr Biol* *17*, 316-322.
- Supek, F., Bosnjak, M., Skunca, N., and Smuc, T. (2011). REVIGO summarizes and visualizes long lists of gene ontology terms. *PLoS ONE* *6*, e21800.
- Taylor, S. S., Hussein, D., Wang, Y., Elderkin, S., and Morrow, C. J. (2001). Kinetochores localisation and phosphorylation of the mitotic checkpoint components Bub1 and BubR1 are differentially regulated by spindle events in human cells. *J Cell Sci* *114*, 4385-4395.
- Westhorpe, F. G., Diez, M. A., Gurden, M. D., Tighe, A., and Taylor, S. S. (2010). Re-evaluating the role of Tao1 in the spindle checkpoint. *Chromosoma* *119*, 371-379.
- Wood, K. W., Lad, L., Luo, L., Qian, X., Knight, S. D., Nevins, N., Brejc, K., Sutton, D., Gilmartin, A. G., Chua, P. R., *et al.* (2010). Antitumor activity of an allosteric inhibitor of centromere-associated protein-E. *Proc Natl Acad Sci U S A* *107*, 5839-5844.
- Yang, W., Soares, J., Greninger, P., Edelman, E. J., Lightfoot, H., Forbes, S., Bindal, N., Beare, D., Smith, J. A., Thompson, I. R., *et al.* (2013). Genomics of Drug Sensitivity in Cancer (GDSC): a resource for therapeutic biomarker discovery in cancer cells. *Nucleic Acids Res* *41*, D955-961.